Article

Cell Reports

A Functional Link between AMPK and Orexin Mediates the Effect of BMP8B on Energy Balance

Graphical Abstract

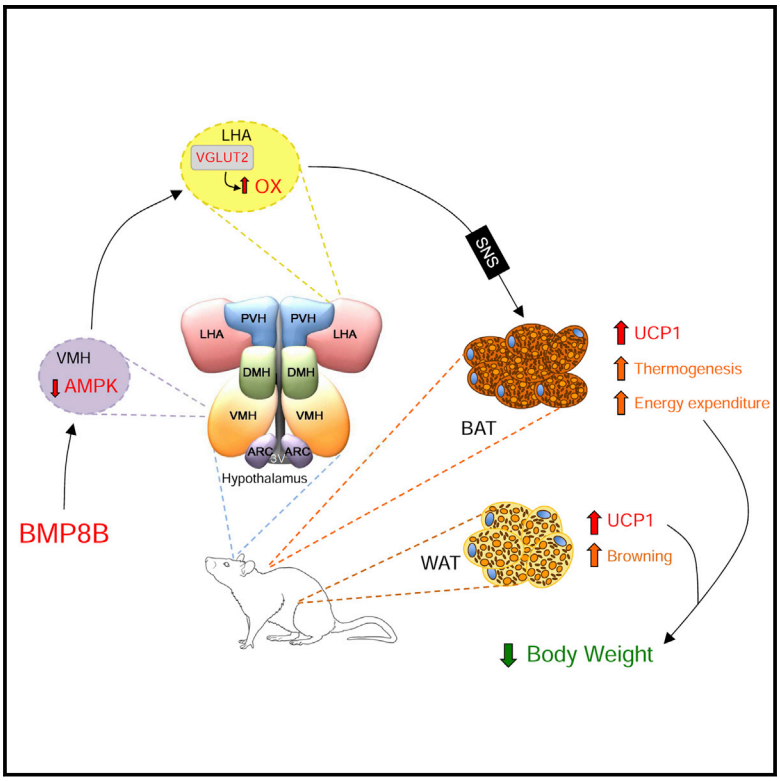

Authors

Luís Martins, Patricia Seoane-Collazo, Cristina Contreras, ..., Rubén Nogueiras, Manuel Tena-Sempere, Miguel López

Correspondence

m.lopez@usc.es

In Brief

Feeding behavior is controlled by two hypothalamic areas: the LHA (the hunger center) and the VMH (the satiety center). Martins et al. demonstrate interplay between orexin in the LHA and AMPK in the VMH, which provides a molecular basis for the regulation of energy expenditure.

Highlights

- Central BMP8B modulates BAT thermogenesis and browning of WAT
- AMPK in the VMH mediates central BMP8B actions
- OX in the LHA mediates central BMP8B actions
- The AMPK(VMH)-OX(LHA) axis is a functional neuronal pathway regulating energy balance

Martins et al., 2016, Cell Reports *16*, 2231–2242
August 23, 2016
http://dx.doi.org/10.1016/j.celrep.2016.07.045

Cell Reports
Article

A Functional Link between AMPK and Orexin Mediates the Effect of BMP8B on Energy Balance

Luís Martins,[1,2,9] Patricia Seoane-Collazo,[1,2,9] Cristina Contreras,[1,2] Ismael González-García,[1,2] Noelia Martínez-Sánchez,[1,2] Francisco González,[3,4] Juan Zalvide,[1] Rosalía Gallego,[5] Carlos Diéguez,[1,2] Rubén Nogueiras,[1,2] Manuel Tena-Sempere,[2,6,7,8] and Miguel López[1,2,10,*]

[1]Department of Physiology, CIMUS, University of Santiago de Compostela-Instituto de Investigación Sanitaria, Santiago de Compostela 15782, Spain
[2]CIBER Fisiopatología de la Obesidad y Nutrición (CIBERobn), Santiago de Compostela 15706, Spain
[3]Department of Surgery, CIMUS, University of Santiago de Compostela-Instituto de Investigación Sanitaria, Santiago de Compostela 15782, Spain
[4]Service of Ophthalmology, Complejo Hospitalario Universitario de Santiago de Compostela, Santiago de Compostela 15706, Spain
[5]Department of Morphological Sciences, School of Medicine, University of Santiago de Compostela-Instituto de Investigación Sanitaria, Santiago de Compostela 15782, Spain
[6]Department of Cell Biology, Physiology and Immunology, University of Córdoba, 14004 Córdoba, Spain
[7]Instituto Maimónides de Investigación Biomédica (IMIBIC)/Hospital Reina Sofía, 14004 Córdoba, Spain
[8]FiDiPro Program, Department of Physiology, University of Turku, Kiinamyllynkatu10, 20520 Turku, Finland
[9]Co-first author
[10]Lead Contact
*Correspondence: m.lopez@usc.es
http://dx.doi.org/10.1016/j.celrep.2016.07.045

SUMMARY

AMP-activated protein kinase (AMPK) in the ventromedial nucleus of the hypothalamus (VMH) and orexin (OX) in the lateral hypothalamic area (LHA) modulate brown adipose tissue (BAT) thermogenesis. However, whether these two molecular mechanisms act jointly or independently is unclear. Here, we show that the thermogenic effect of bone morphogenetic protein 8B (BMP8B) is mediated by the inhibition of AMPK in the VMH and the subsequent increase in OX signaling via the OX receptor 1 (OX1R). Accordingly, the thermogenic effect of BMP8B is totally absent in *ox*-null mice. BMP8B also induces browning of white adipose tissue (WAT), its thermogenic effect is sexually dimorphic (only observed in females), and its impact on OX expression and thermogenesis is abolished by the knockdown of glutamate vesicular transporter 2 (VGLUT2), implicating glutamatergic signaling. Overall, our data uncover a central network controlling energy homeostasis that may be of considerable relevance for obesity and metabolic disorders.

INTRODUCTION

Hypothalamic neural circuits are involved in the control of a large number of functions, the regulation of endocrine axes and energy balance being of particular importance (Yeo and Heisler, 2012; Schneeberger et al., 2014; López et al., 2016). Substantial interest and efforts have been devoted to the analysis of the arcuate nucleus of the hypothalamus (ARC), which, in fact, has been considered as the master hypothalamic center for energy homeostasis (Yeo and Heisler, 2012; Schneeberger et al., 2014; López et al., 2016). Despite this evidence, other hypothalamic sites, such as the ventromedial nucleus of the hypothalamus (VMH), formerly characterized as the brain satiety center, and the lateral hypothalamic area (LHA), formerly characterized as the brain hunger center (Hecherington and Ranson, 1942; Anand and Brobeck, 1951), also play major and probably more integrative roles than the ARC in the modulation of energy balance. These regions receive information from ARC neurons and also project their axons to other hypothalamic and extra-hypothalamic sites (Schneeberger et al., 2014; Contreras et al., 2015; López et al., 2016) to control not only feeding but also several peripheral processes, such as adipose and hepatic metabolism, as well as brown adipose tissue (BAT) thermogenesis through the sympathetic (SNS) and parasympathetic nervous system (PSNS) (Nogueiras et al., 2007; Fliers et al., 2010; Stanley et al., 2010; Imbernon et al., 2013; López et al., 2013, 2016).

The molecular mediators within those areas have begun to be characterized, and over the last 5 years extensive attention has been focused on the role of AMP-activated protein kinase (AMPK) in the VMH and orexin (OX) in the LHA as key modulators of brown fat. Thus, inhibition of AMPK function in the VMH (López et al., 2010b, 2016; Martínez de Morentin et al., 2012, 2014; Whittle et al., 2012; Tanida et al., 2013; Beiroa et al., 2014) or increased orexigenic tone in the LHA (Teske et al., 2006; Tupone et al., 2011; Morrison et al., 2012; Madden et al., 2012) activates the BAT thermogenic program, leading to elevated temperature, increased energy expenditure (EE), and weight loss. In addition, OX neurons in the LHA are required for BAT development and differentiation (Sellayah et al., 2011; Sellayah and Sikder, 2012, 2014). In spite of this evidence, no functional data have linked those neuronal populations, and it is currently unknown whether AMPK in the VMH and OX neurons in the LHA are part of the

same circuit modulating BAT function or, alternatively, they function separately.

Bone morphogenetic proteins (BMPs) belong to the transforming growth factor β (TGF-β) superfamily. BMPs regulate a wide range of processes from embryonic development to tissue homeostasis (Schulz and Tseng, 2009; Modica and Wolfrum, 2013). Among these functions, BMPs also are involved in adipocyte development. BMP2 and -4 and BMP7 and -9 were identified as important elements in white and brown adipocyte differentiation, respectively (Tang et al., 2004; Bowers et al., 2006; Huang et al., 2009; Kuo et al., 2014). In addition, a more recent report has shown that BMP4 induces brown adipocyte characteristics in mature white adipocytes (Qian et al., 2013). Other recent findings, including those from our group, surfaced a role for BMPs in energy balance. Thus, BMP7 and BMP8B were demonstrated to regulate BAT thermogenic function and increase EE (Tseng et al., 2008; Townsend et al., 2012, 2013; Whittle et al., 2012). Given that BMP8B acts centrally, its thermogenic effect is dependent upon the activation status of AMPK in the VMH, and it increases neuronal activation in the LHA (Whittle et al., 2012), we aimed to uncover the neuronal circuitry linking energy sensors and neuropeptides involved in the thermogenic effect of central BMP8B.

RESULTS

The Thermogenic Effect of Central BMP8B Is Sexually Dimorphic

Recent evidence has demonstrated that central BMP8B exerts a robust thermogenic effect in females (Whittle et al., 2012). Thus, we aimed to investigate whether males had a similar response. Our data showed that after 2 hr of an intracerebroventricular (i.c.v.) injection of BMP8B, male rats did not show an increase in either body (Figure 1A) or BAT temperature (Figure 1B).

Next we analyzed the effect of central BMP8B in ovariectomized (OVX) female rats with and without estradiol (E2) replacement and their sham-operated controls (Martínez de Morentin et al., 2014, 2015). OVX rats gained significantly more weight (sham: 23.1 ± 2.38 g versus OVX: 71.3 ± 28 g; $p < 0.001$) and developed a marked hyperphagia (sham: 14.87 ± 0.31 g/day versus OVX: 17.70 ± 0.49 g/day; $p < 0.01$), confirming the efficiency of the OVX procedure. While central administration of BMP8B to sham controls induced a clear thermogenic action, OVX totally abolished it at both body and BAT temperature levels. Of note, OVX rats with E2 replacement responded normally to BMP8B (Figures 1C and 1D). Overall, these data indicated that the thermogenic action of BMP8B shows a sexual dimorphism and depends on physiological levels of ovarian estrogens.

The Thermogenic Effect of Central BMP8B Is Independent of Environmental Temperature

We aimed to investigate whether the thermogenic central actions of BMP8B were affected by temperature. Therefore, we administered central BMP8B to female rats kept at 23°C or 4°C during 10 hr prior to the i.c.v. treatment and for a total of 12 hr. Our data showed that BMP8B protected against the loss of both core (Figure 1E) and BAT (Figure 1F) temperature when given at 4°C.

BMP8B in the VMH, but Not in the LHA, Induces Negative Energy Balance

To investigate the effect of chronic nucleus-specific BMP8B treatment, stereotaxic cannulae were placed in the VMH and the LHA. The correct position of the cannulae was verified by histological examination of coronal sections of the brains (Figures S1A and S1B). Noteworthy, the expression of BMP type I receptors ALK4, ALK5, and ALK7 in those nuclei was demonstrated by real-time RT-PCR analysis (Figure S2A) of dissected VMH and LHA, whose specificity was controlled by analysis of the specific markers steroidogenic factor 1 (SF1) and OX, respectively (Figure S2B).

When given in the VMH, BMP8B promoted a feeding-independent weight loss (Figure 2A; initial body weight vehicle VMH: 240.0 ± 4.4 g versus BMP8B VMH: 237.5 ± 4.0 g; non-significant); no effect was observed when BMP8B was injected in the LHA (Figure 2B; initial body weight vehicle LHA: 233.0 ± 3.1 g versus BMP8B LHA: 235.1 ± 1.8 g; non-significant). The action of BMP8B in the VMH was associated with a trend ($p = 0.07$) to reduce adiposity without changes in the lean mass (Figure 2C). BMP8B in the LHA promoted no changes either in fat or lean mass (Figure 2D).

BMP8B in the VMH, but Not in the LHA, Increases Temperature and EE

Treatment with BMP8B within the VMH induced a marked elevation in body temperature, which was consistent during the whole period of administration (Figure 2E). No effect on body temperature was found when BMP8B was given in the LHA (Figure 2F). Moreover, BMP8B in the VMH, but not in the LHA, increased EE (Figures 2G and 2H) and reduced the respiratory quotient (RQ; Figures 2I and 2J). No changes in locomotor activity (LA) were found when BMP8B was administered either in the VMH or the LHA (Figures 2K and 2L), although a non-significant trend ($p = 0.07$) for increased LA was detected in VMH BMP8B-treated rats.

BMP8B in the VMH, but Not in the LHA, Regulates Hypothalamic AMPK, the Expression of Thermogenic Markers in BAT, and Browning of WAT

We aimed to investigate whether hypothalamic nucleus-specific BMP8B actions result in changes in AMPK signaling within the VMH. We found that VMH administration of BMP8B decreased the phosphorylated levels of AMPKα (pAMPKα) and its downstream target acetyl-CoA carboxylase alpha (pACCα); no changes were found in total levels of AMPKα1, AMPKα2, ACCα, and fatty acid synthase (FAS) (Figure 3A). BMP8B within the VMH also increased UCP1 protein levels (Figure 3B) and the mRNA expression of thermogenic markers (Figure 3C) in the brown fat. When administered in the LHA, BMP8B did not affect either AMPK signaling in the VMH (Figure 3D) or UCP1 protein levels (Figure 3E) or the mRNA expression of thermogenic markers (Figure 3F) in the BAT. This evidence suggests that BMP8B's actions on the VMH are direct and not mediated by a previous effect on the LHA.

In relation to the white adipose tissue (WAT), our mRNA data showed that browning markers had a tendency to be increased in the WAT of rats receiving BMP8B in the VMH, but not in the LHA (Figures 3G and 3I). Histological analysis of WAT showed

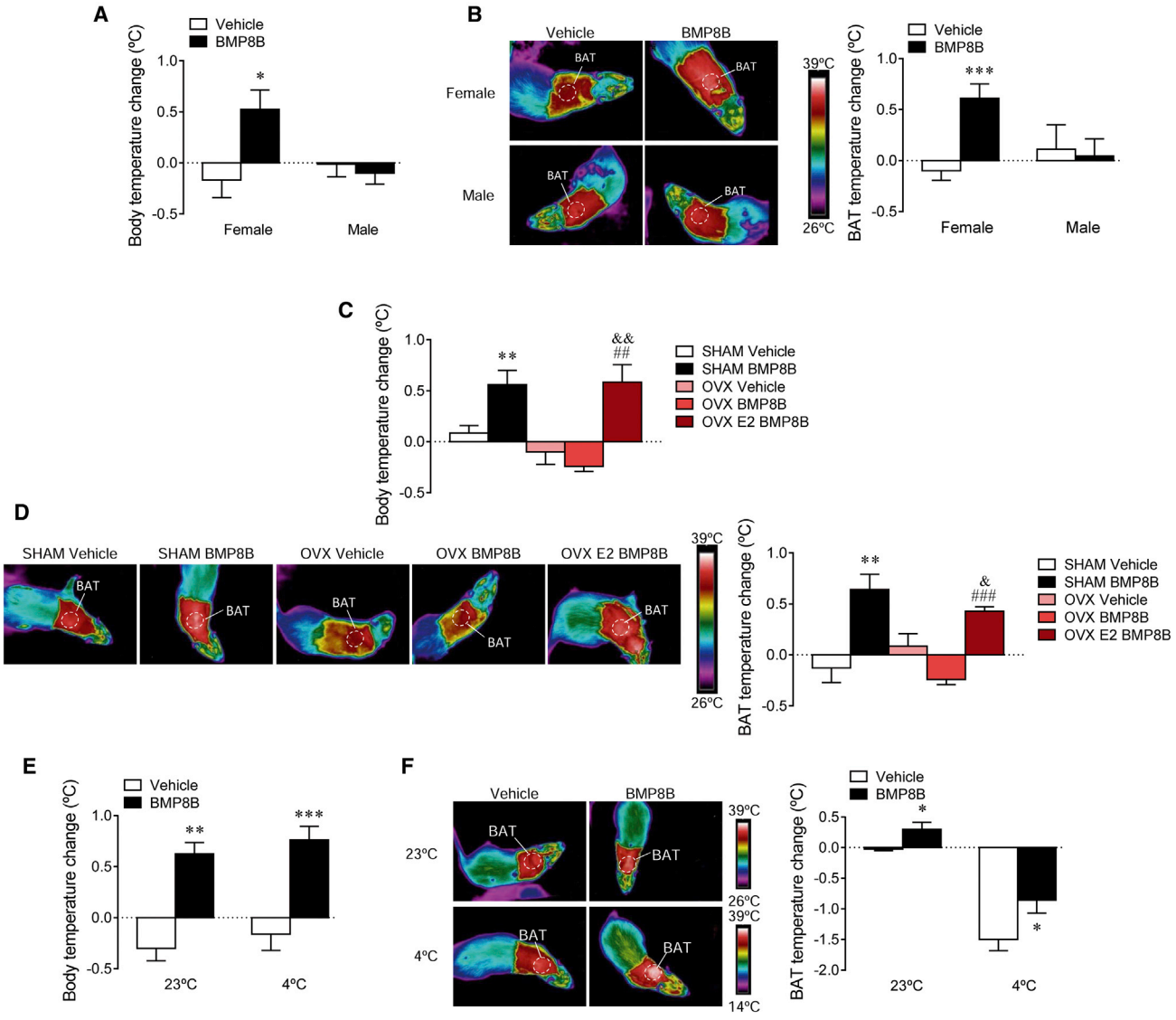

Figure 1. Effect of i.c.v. Administration of BMP8B on Energy Balance

(A and B) Body temperature change (A) and thermal images (B, left panel) and quantification of temperature change in the skin surrounding BAT (right panel) of female and male rats receiving i.c.v. administration of BMP8B or vehicle. Experiments were repeated twice and total animals per experimental group was n = 6–18.

(C and D) Body temperature change (C) and thermal images (D, left panel) and quantification of temperature change in the skin surrounding BAT (right panel) of sham and OVX with and without E2 replacement rats receiving i.c.v. administration of BMP8B or vehicle. Experiments were repeated twice and total animals per experimental group was n = 12–15.

(E and F) Body temperature change (E) and thermal images (F, left panel) and quantification of temperature change in the skin surrounding BAT (right panel) of female rats exposed to 23°C or 4°C during 12 hr and receiving i.c.v. administration of BMP8B or vehicle. Experiments were repeated twice and total animals per experimental group was n = 10–16. For each set of data a representative experiment is shown. Data are expressed as mean ± SEM (*p < 0.05, **p < 0.01, and ***p < 0.001 versus vehicle [female vehicle and sham vehicle]; &p < 0.05 and &&p < 0.01 versus OVX vehicle; and ##p < 0.01 and ###p < 0.001 versus OVX BMP8B). Temperature changes were calculated versus basal values.

that BMP8B-treated rats in the VMH displayed a brown-like pattern, associated with increased UCP1 immunostaining and decreased adipocyte area (Figure 3H). No changes were found when BMP8B was given in the LHA (Figure 3J). Overall, these data indicated that the effects of BMP8B on browning are specific for the VMH.

Central BMP8B Increases OX Expression in the LHA through AMPK in the VMH

Recent data have demonstrated a key role for OX on BAT thermogenic activity (Tupone et al., 2011; Sellayah et al., 2011; Morrison et al., 2012; Madden et al., 2012; Sellayah and Sikder, 2012, 2014). Furthermore, it has been reported that central administration of

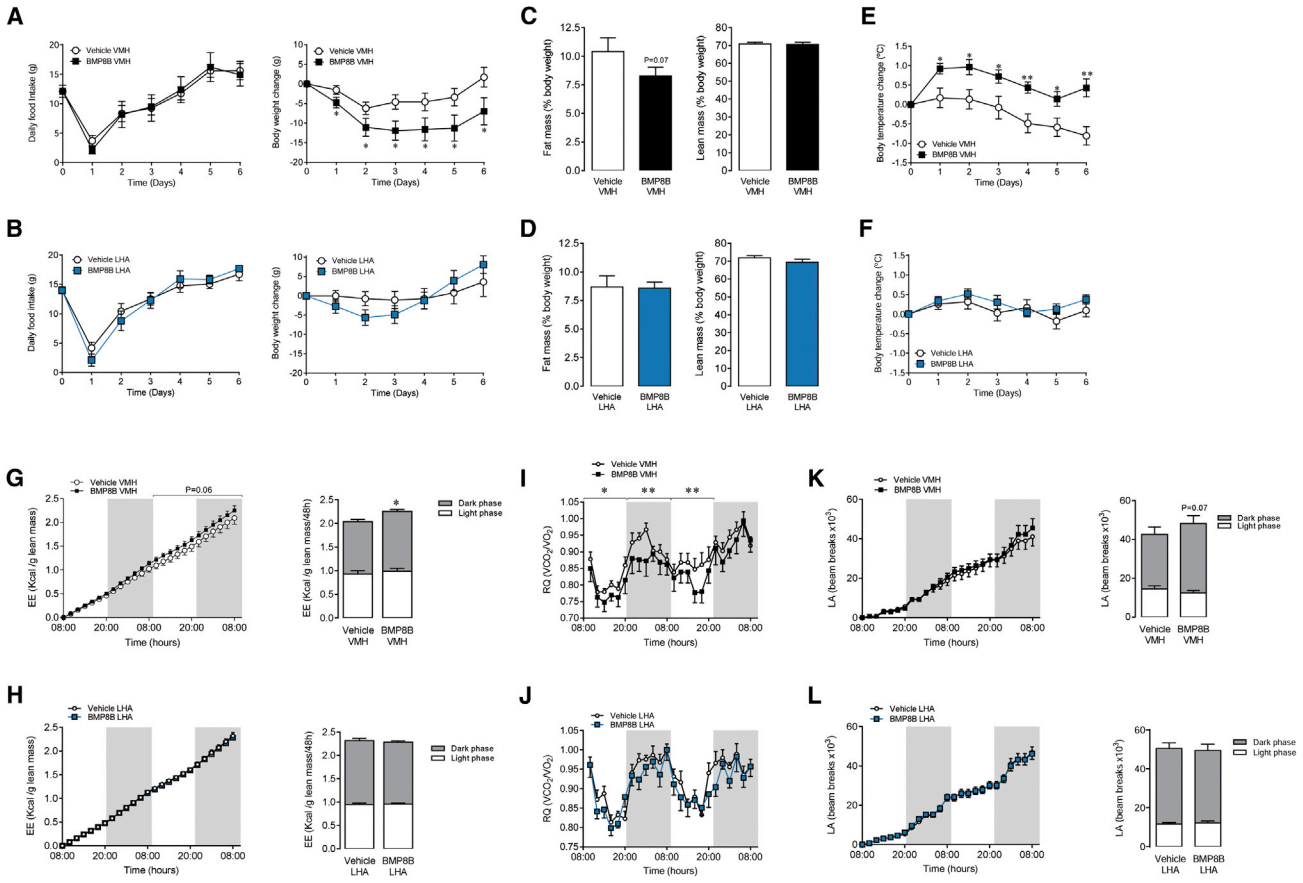

Figure 2. Effect of Stereotaxic Administration of BMP8B on Energy Balance

(A–L) The following are shown: (A and B) daily food intake (left panel) and body weight change (right panel), (C and D) fat mass (left panel) and lean mass (right panel), (E and F) body temperature change, (G and H) energy expenditure (EE; left panel cumulative, right panel total), (I and J) respiratory quotient (RQ), and (K and L) locomotor activity (LA; left panel cumulative, right panel total) of rats receiving chronic stereotaxic administration of vehicle or BMP8B in the VMH (A, C, E, G, I, and K) or the LHA (B, D, F, H, J, and L). Data are expressed as mean ± SEM (n = 8–16 animals per experimental group; *p < 0.05 and **p < 0.01 versus vehicle VMH). Temperature changes were calculated versus basal values.

BMP8B increased neuronal activity in the LHA (Whittle et al., 2012), the main hypothalamic area expressing OX. Thus, we investigated the possible effect of BMP8B on OX expression in the LHA. Our data showed that i.c.v. administration of BMP8B increased body temperature (vehicle i.c.v.: −0.1°C ± 0.09°C versus BMP8B i.c.v.: 0.48°C ± 0.07°C; $p < 0.001$) and UCP1 protein levels in BAT (vehicle i.c.v.: 100% ± 14.6% versus BMP8B i.c.v.: 137.8% ± 10.1%; $p < 0.05$), in association with elevated OX mRNA expression in the LHA (Figure S3A).

To gain further insight into BMP8B effects on OX expression, we analyzed the effect of specific administration of BMP8B in the VMH. Our data showed that, when given in that nucleus, BMP8B also increased the mRNA levels of OX in the LHA (Figure 4A). These results suggested that BMP8B in the VMH acts upstream in the LHA to promote OX expression. To elucidate the contribution of AMPK activity in the VMH to the thermogenic effect of BMP8B, adenoviruses encoding constitutively active AMPKα (AMPKα-CA) together with GFP or control adenovirus expressing GFP alone (López et al., 2010b; Whittle et al., 2012; Martínez de Morentin et al., 2012, 2014; Beiroa et al., 2014) were injected stereotaxically into the VMH of rats centrally treated with vehicle or BMP8B. Infection efficiency was assessed by the expression of GFP in the VMH (Figure 4B). The administration of AMPKα-CA adenoviruses alone did not have any impact either in body temperature change (vehicle GFP: 0.37°C ± 0.14°C versus vehicle AMPKα-CA: 0.3°C ± 0.11°C, non-significant) or BAT temperature (vehicle GFP: 0.35°C ± 0.21°C versus vehicle AMPKα-CA: 0.29°C ± 0.15°C, non-significant). When given to BMP8B-treated rats, constitutive activation of AMPK in the VMH reversed the thermogenic effect of BMP8B at both whole body (Figure 4C) and BAT levels (Figure 4D). This effect also was associated with a reduction in the expression of OX in the LHA (Figure 4E). These results suggest that central BMP8B action on OX expression is mediated by the inhibition of AMPK in the VMH.

OX1R Antagonism Reversed the Thermogenic Effect of Central BMP8B

It has been reported recently that OX1R mediates OX actions on BAT function (Sellayah and Sikder, 2012). Thus, rats

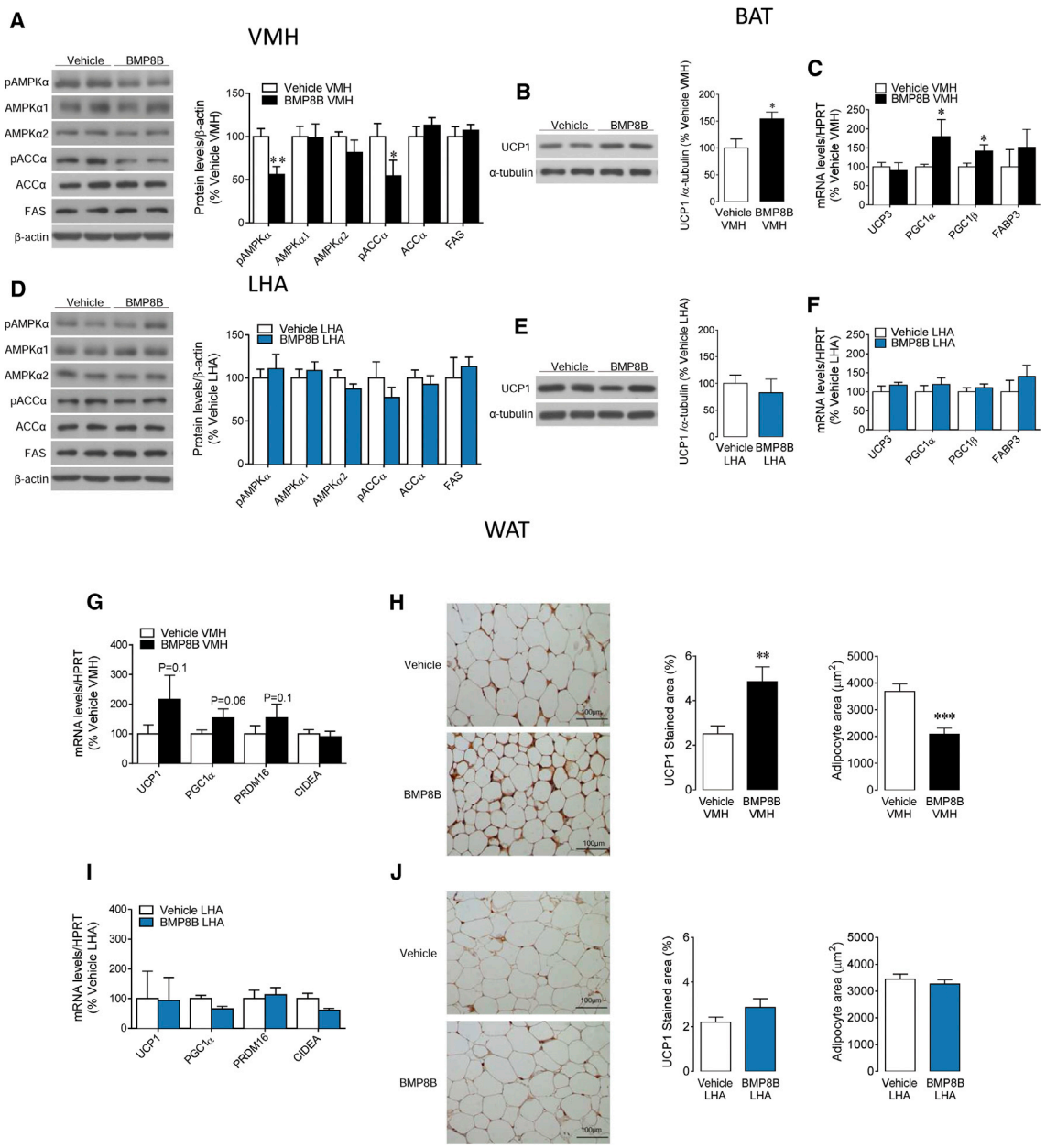

Figure 3. Effect of Stereotaxic Administration of BMP8B on Hypothalamic AMPK, BAT UCP1, and Browning of WAT

(A–J) The following are shown: (A and D) western blot images (left panel) and protein levels of the AMPK pathway (right panel); (B and E) western blot images (left panel) and UCP1 protein levels in BAT (right panel); (C and F) mRNA expression of thermogenic markers in BAT; (G and I) mRNA expression of browning markers in WAT; and (H and J) microphotographs of WAT showing UCP1 immunostaining (left panel), quantification of UCP1 staining (middle panel), and adipocyte area (right panel) of rats receiving chronic stereotaxic administration of vehicle or BMP8B in the VMH (A–C, G, and H) or the LHA (D–F, I, and J). Data are expressed as mean ± SEM (n = 8–9 animals per experimental group; *p < 0.05, **p < 0.01, and ***p < 0.001 versus vehicle VMH).

received the OX1R antagonist SB-334867 (Jia et al., 2012) 30 min prior to BMP8B administration. SB-334867 alone had no effect on body temperature at any examined time (2 hr vehicle vehicle: 0.19°C ± 0.08°C versus vehicle SB-334867: 0.20 ± 0.07, non-significant; 4 hr vehicle vehicle: 0.40°C ± 0.14°C versus vehicle SB-334867: 0.39 ± 0.17, non-significant; and 6 hr vehicle vehicle: 0.26°C ± 0.13°C versus vehicle SB-334867: 0.23 ± 0.19, non-significant). However, SB-334867 significantly blunted the thermogenic effect of BMP8B at 4 and 6 hr after BMP8B treatment but only partially at 2 hr (Figure 4F), probably due to early effects independent of OX1R or a delayed effect of the antagonist. Of note, SB-334867 did not have any impact on the BMP8B-induced decrease in AMPK signaling in the VMH (Figure 4G), suggesting that AMPK in that nucleus operates upstream of OX1R signaling in this pathway.

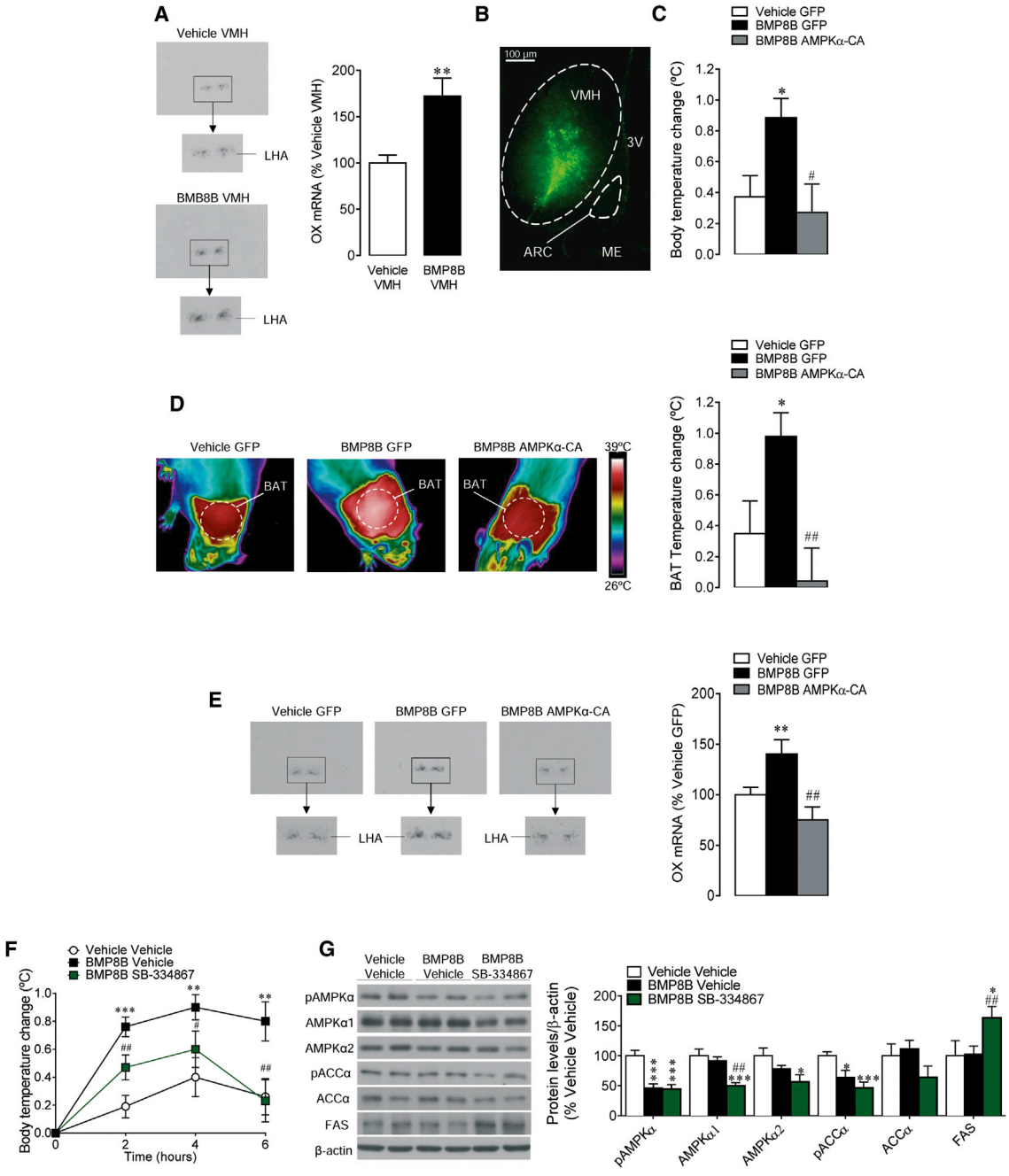

Figure 4. Effect of BMP8B in the VMH on OX System

(A) In situ hybridization images (left panel) and OX mRNA levels in the LHA (right panel) of rats receiving chronic stereotaxic administration of BMP8B or vehicle in the VMH are shown.

(B) Representative immunofluorescence (20×) with anti-GFP antibody showing GFP expression in the VMH of rats treated with adenoviruses within the VMH, is shown.

(C–E) The (C) quantification of body temperature change, (D) thermal images (left panel) and quantification of temperature change in the skin surrounding BAT (right panel), and (E) in situ hybridization images (left panel) and OX mRNA levels in the LHA (right panel) of rats i.c.v. treated with vehicle or BMP8B and stereotaxically treated with GFP or AMPKα-CA adenoviruses within the VMH are shown.

(F and G) The (F) body temperature change and (G) western blot images (left panel) and protein levels of the AMPK pathway (right panel) of rats i.c.v. treated with vehicle or BMP8B and i.c.v. treatment with the OX1R antagonist SB-334867. Data are expressed as mean ± SEM (n = 8–12 animals per experimental group for the AMPKα-CA experiments, n = 30–40 animals per experimental group for the temperature analysis, and n = 8 animals per experimental group for the western blot analysis for the SB-334867 experiments; *p < 0.05, **p < 0.01, and ***p < 0.001 versus vehicle VMH, vehicle GFP, or vehicle vehicle; #p < 0.05 and ##p < 0.01 versus BMP8B GFP or BMP8B vehicle). Temperature changes were calculated versus basal values. 3V, third ventricle; ME, median eminence.

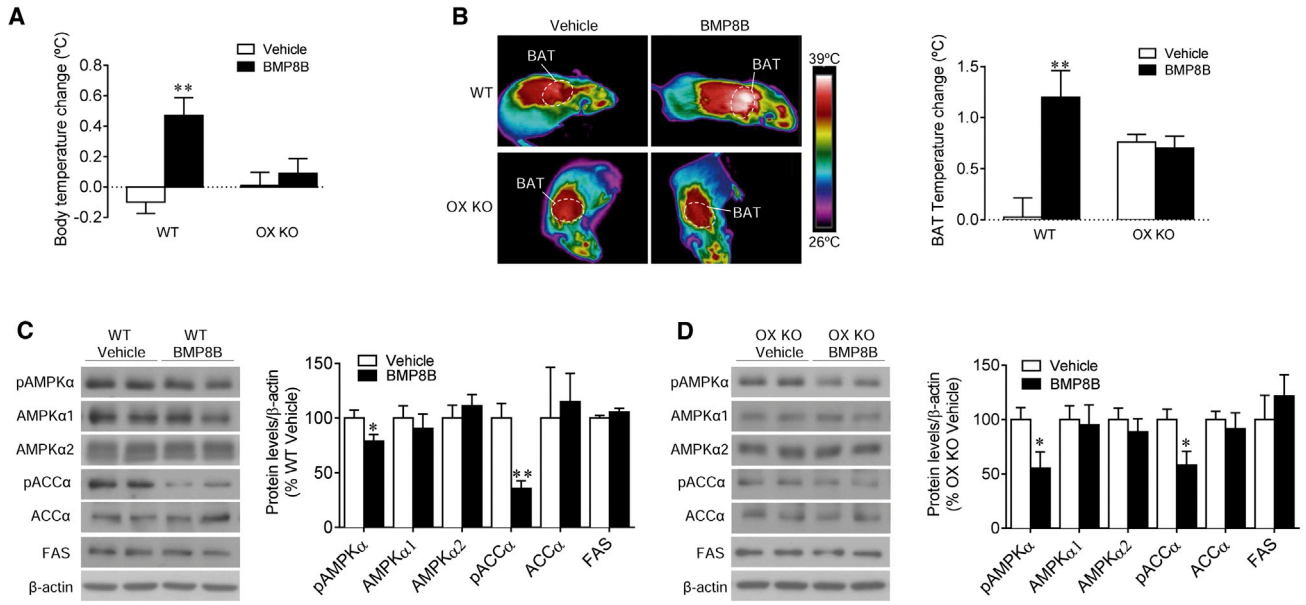

Figure 5. Effect of OX Deficiency on BMP8B Action

(A–D) The (A) body temperature change, (B) thermal images (left panel) and quantification of temperature change of the skin surrounding BAT (right panel), and (C and D) western blot images (left panel) and VMH protein levels of the AMPK pathway (right panel) of *Ox*-null mice (OX KO) and their WT littermates, i.c.v. treated with vehicle or BMP8B. Data are expressed as mean ± SEM (n = 11–13 animals per experimental group; *p < 0.05 and **p < 0.01 versus vehicle). Temperature changes were calculated versus basal values.

OX Mediates the Thermogenic Effect of Central BMP8B Independently of Environmental Temperature

Afterward, we examined the effect of BMP8B on *Ox*-null mice and their wild-type (WT) littermates. When given centrally, BMP8B increased body temperature (Figure 5A) and BAT temperature (Figure 5B) in WT, but not in OX knockout (KO) mice. Notably, AMPK signaling was decreased in the VMH of both WT (Figure 5C) and OX KO mice (Figure 5D), suggesting again that AMPK in the VMH is upstream of OX in the LHA.

We also investigated whether the effect of OX on BMP8B-induced thermogenesis was dependent on temperature. Our data showed that null mice were cold intolerant when exposed to 4°C for just 12 hr (Figure 6A). Next we analyzed the effect of i.c.v. BMP8B on WT and OX KO animals at 23°C and 4°C. Our data demonstrated that, while WT mice kept at 4°C had a full thermogenic response to central BMP8B (similarly to rats; Figures 1E and 1F), OX KO mice failed to respond (Figures 6B and 6C). Those effects were associated with a similar effect in the VMH in both genotypes, i.e., reduced pAMPK levels, after the i.c.v. injection of BMP8B (Figures 6D and 6E). However, accordingly with the temperature data, while WT mice displayed elevated UCP1 protein levels in BAT (Figure 6F), KO mice did not (Figure 6G). Again, these data reinforced the ideas that the VMH-LHA circuit is essential for the central actions of BMP8B on BAT and that OX acts downstream of AMPK in the VMH.

Glutamatergic Signaling Mediates the Thermogenic Effect of Central BMP8B

Finally, we aimed to investigate the cellular mechanism through which BMP8B mediates increased OX expression in the LHA. It is known that glutamate and glutamate transporters, particularity glutamate vesicular transporter 2 (VGLUT2), play a main role in hypothalamic regulation of energy balance (Tong et al., 2007). Therefore, we investigated whether virogenetic targeting of VGLUT2 within the LHA, by using lentiviruses harboring a small hairpin RNA (shRNA) against VGLUT2 (or their GFP controls), might reverse the effects of BMP8B on OX expression. Infection efficiency was assessed by decreased VGLUT2 levels in that area (Figure 7A). Our data showed that shVGLUT2 lentiviruses totally blunted central BMP8B effects on both core and BAT temperatures (Figures 7B and 7C). Those functional readouts were associated with a normalization in the BMP8B-induced increase in OX mRNA levels in the LHA (Figure 7D) and UCP1 protein concentration in the BAT (Figures 7E and 7F). Of note, pAMPK protein levels were reduced in both the GFP- and the shVGLUT2-treated groups (vehicle GFP: 100 ± 18.6 versus BMP8B GFP: 42.6 ± 12.3, $p < 0.05$; and vehicle shVGLUT2: 100 ± 10.7 versus BMP8B shVGLUT2: 62.9 ± 12.5, $p < 0.05$), indicating that glutamatergic signaling was acting downstream of AMPK.

DISCUSSION

Here, we report a functional link between AMPK in the VMH and OX neurons in the LHA. Moreover, we show that the thermogenic effect of BMP8B is mediated by the inhibition of AMPK in the VMH, the glutamatergic signaling in the LHA, and the subsequent increase in OX signaling through OX1R.

BAT is a specialized tissue responsible for heat production through non-shivering thermogenesis (NST) (Cannon and

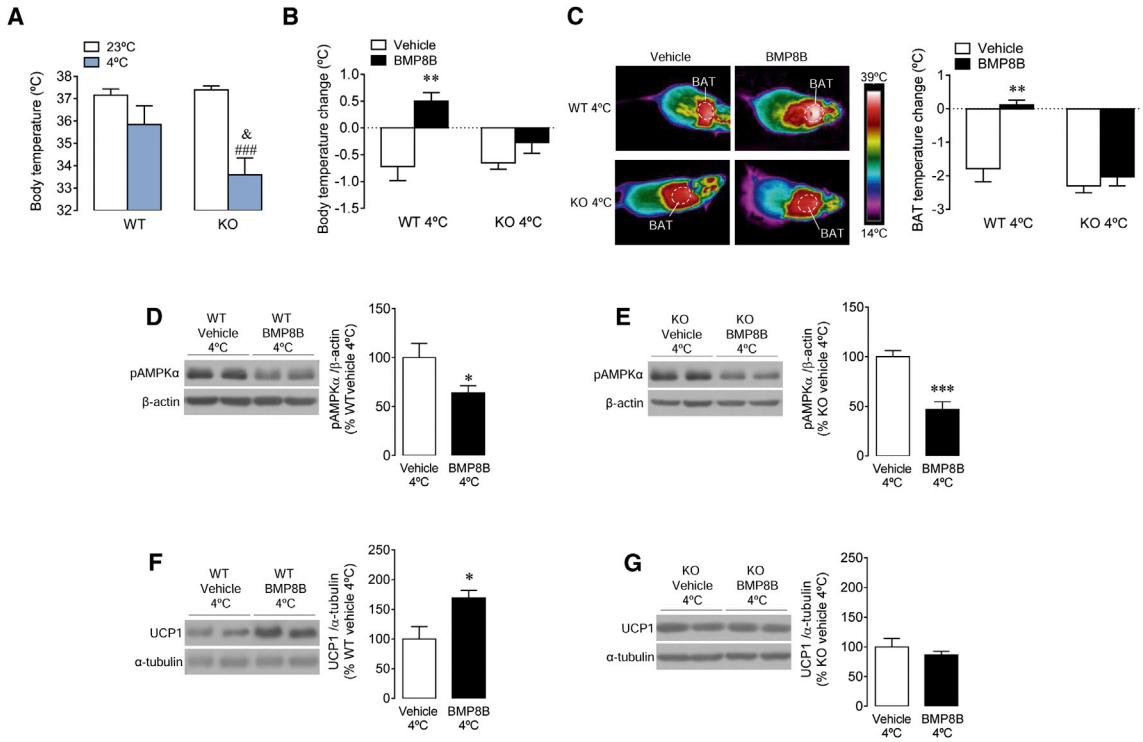

Figure 6. Effect of OX Deficiency and Cold on BMP8B Action

(A) Body temperatures of *Ox*-null mice (OX KO) and their WT littermates exposed to 23°C or 4°C are shown.

(B–G) The (B) body temperature change, (C) thermal images (left panel) and quantification of temperature change of the skin surrounding BAT (right panel), (D and E) western blot images (left panel) and VMH pAMPKα protein levels (right panel), and (F and G) western blot images (left panel) and BAT UCP1 protein levels (right panel) of *Ox*-null mice (OX KO) (B, C, E, and G) and their WT littermates (B–D and F) i.c.v. treated with vehicle or BMP8B and exposed to cold for 12 hr. Data are expressed as mean ± SEM (n = 6–12 animals per experimental group; *p < 0.05, **p < 0.01, and ***p < 0.001 versus vehicle; ###p < 0.001 versus KO 23°C; and &p < 0.05 versus WT 4°C). Temperature changes were calculated versus basal values.

Nedergaard, 2004; Morrison et al., 2014; Contreras et al., 2015). Until recently, BAT was considered to be important only in small or hibernating mammals and in newborn humans. Recent studies have challenged that view by using positron emission tomography-computed tomography (PET-CT) scans to identify functional BAT in adult humans (Nedergaard et al., 2007; Cypess et al., 2009; Virtanen et al., 2009; van Marken Lichtenbelt et al., 2009), and brown fat is now considered as a potential target organ in the treatment of obesity (Villarroya and Vidal-Puig, 2013; Contreras et al., 2015). The CNS controls BAT function through the SNS. BAT is activated by increased firing of the sympathetic nerves, leading to the release of noradrenaline and activation on β3-adrenergic receptors (Cannon and Nedergaard, 2004; Contreras et al., 2015; López et al., 2016).

Recent data have demonstrated that central BMP8B elicits BAT thermogenesis in females through modulation of hypothalamic AMPK (Whittle et al., 2012). Of note, this mechanism is shared by E2, which also displays a potent central thermogenic action (Martínez de Morentin et al., 2014, 2015). Here we show that male rats did not respond to central BMP8B administration, which might indicate dependence on ovarian steroids, a possibility that was further confirmed by using OVX rats with and without E2 replacement. This is of relevance because it indicates that BMP8B actions are sexually dimorphic. In this sense, it has been reported that BMP8B expression in BAT is regulated by estrogens (Grefhorst et al., 2015). Further work analyzing E2 effects in BMP8B KO mice (Whittle et al., 2012) will help to clarify this issue.

Within the hypothalamus, the VMH was the first hypothalamic site to be identified as important in BAT thermogenic action (Perkins et al., 1981). Anatomical data also have demonstrated that VMH neurons project to autonomic centers in the hypothalamus and the hindbrain linked to the regulation of BAT (Lindberg et al., 2013). Recent evidence has revealed that particular sets of cells within the VMH, such as SF1 neurons (Kim et al., 2011; Xu et al., 2011), and specific energy sensors, such as AMPK (López et al., 2010b, 2016; Martínez de Morentin et al., 2012, 2014; Whittle et al., 2012; Tanida et al., 2013; Beiroa et al., 2014), control the sympathetic firing on BAT to regulate thermogenesis and browning of WAT (Beiroa et al., 2014). The LHA, containing OX neurons, also is involved in thermoregulation and EE. Activation of the LHA promotes BAT function (Cerri and Morrison, 2005), and compelling evidence has shown that this effect is mediated by OX acting on OX1R and involving direct projections from the LHA to the raphe pallidus (RPa), a key area modulating the sympathetic tone to brown fat (Yasuda et al., 2005; Sellayah et al., 2011; Tupone et al., 2011; Madden et al., 2012; Sellayah and Sikder, 2012, 2014).

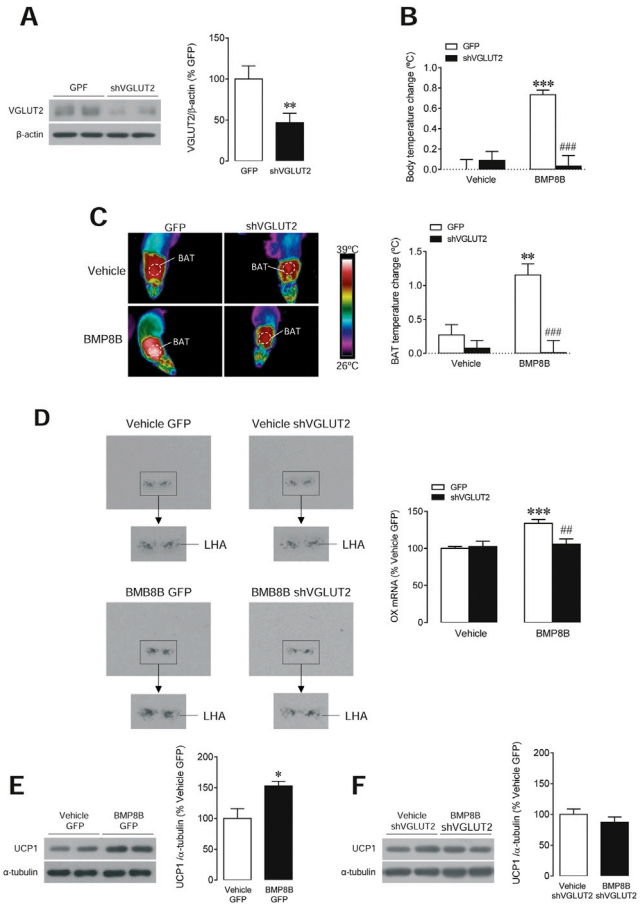

Figure 7. Effect of Stereotaxic Administration of shVGLUT2 in the LHA on BMP8B Action

(A–F) The (A) western blot images (left panel) and LHA VGLUT2 protein levels, (B) body temperature change, (C) thermal images (left panel) and quantification of temperature change of the skin surrounding BAT (right panel), (D) in situ hybridization images (left panel) and OX mRNA levels in the LHA (right panel), and (E and F) western blot images (left panels) and BAT UCP1 protein levels of rats treated i.c.v. with vehicle or BMP8B and stereotaxically treated with GFP or shVGLUT2 lentiviruses within the LHA. Data are expressed as mean ± SEM (n = 6–9 animals per experimental group; *p < 0.05, **p < 0.01, and ***p < 0.001 versus GFP (A) or vehicle GFP (E); ##p < 0.01 and ###p < 0.001 versus BMP8B GFP). Temperature changes were calculated versus basal values.

In spite of this evidence, it was totally unclear whether AMPK in the VMH and OX in the LHA are part of the same functional link or they exert their thermogenic actions separately. Anatomical data supported the hypothesis of an interconnected pathway, because it was known that VMH efferents project to the LHA and provide passing innervation on their way to their target areas (Lindberg et al., 2013). To address that possibility, we investigated the central thermogenic effect of BMP8B, which is associated with (1) decreased AMPK function in the VMH; (2) increased activity in RPa, inferior olive (IO), and sympathetic tone; and (3) neuronal activation within the LHA (Whittle et al., 2012). Our data showed that administration of BMP8B within the VMH recapitulated the effect of its central (i.c.v.) administration (Whittle et al., 2012), namely feeding-independent weight loss, increased EE and BAT thermogenesis, and reduced RQ, in association with reduced AMPK signaling in the VMH and elevated BAT UCP1 protein content as well as browning of WAT. None of these outcomes was observed when BMP8B was specifically delivered into the LHA, which excluded its direct effect at this level.

Interestingly, the thermogenic effect of both central and VMH-specific BMP8B administration correlated with increased OX expression in the LHA. Considering that OX also is known to stimulate thermogenesis through the RPa-SNS route (Tupone et al., 2011), we investigated its potential link with the BMP8B-AMPK pathway. We observed that both the thermogenic effect of BMP8B and the elevation of OX mRNA expression were totally absent when BMP8B was given in combination with adenoviral particles encoding AMPKα-CA, indicating that AMPK in the VMH was acting upstream of OX neurons in the LHA. Importantly, the above effects were reversed by pharmacological blockage of OX1R and were totally absent when BMP8B was centrally delivered in OX KO mice, even in a cold environment, which confirmed again AMPK's upstream position in this network.

To gain further insight into this central pathway, we investigated the cellular mechanism regulating OX expression by BMP8B. It is known that glutamate transporters, particularity VGLUT2, are highly expressed in the hypothalamus, including OX neurons (Ziegler et al., 2002; Rosin et al., 2003), and play a main role in the regulation of energy balance (Tong et al., 2007). Therefore, we hypothesized a possible link with BMP8B effects on OX neurons in the LHA. To check that possibility, we knocked down VGLUT2 in the LHA using lentiviruses harboring an shRNA. Notably, VGLUT2 inhibition totally blunted BMP8B's effects on temperature, OX expression in the LHA, and UCP1 expression in BAT. Whether VGLUT2 in AMPK-expressing neurons mediates this effect is unclear. However, it has been revealed recently, by using conditional viral tracing, that SF1 neurons, a major cell population inside the VMH, project and terminate in the LHA (Lindberg et al., 2013), which may provide an anatomical basis for the interaction of AMPK(VMH)-glutamate-OX(LHA).

These results are of relevance for several reasons. First, they uncover a physiological hypothalamic network governing energy homeostasis, which might be of relevance for therapeutic approaches. In this sense, it is important to highlight that the original theories explaining the central control of energy balance were based on a Dual Centre Hypothesis (Hecherington and Ranson, 1942; Anand and Brobeck, 1951). In that model, feeding was controlled by two hypothalamic areas: the LHA hunger center and the VMH satiety center. Lesions of the LHA decreased food intake and eventually led to starvation and death. Conversely, lesions of the VMH (and the neighboring mediobasal area) resulted in obesity. The present results do not show an impact on feeding, but this VMH (AMPK), glutamate and LHA (OX) pathway provides the molecular basis for the interplay and balance between these two major areas in the dynamic control of other key aspect of the energy balance equation, namely EE. Second, the sexual dependency of the thermogenic effect of BMP8B, and in particular the relevance of endogenous ovarian steroids in the modulation of BMP8B thermogenic actions, might be of clinical relevance, considering the different

thermogenic adaptation observed in women and men (Palmer and Clegg, 2015; Mauvais-Jarvis, 2015). Third, OXs are highly pleiotropic peptides (Tsujino and Sakurai, 2009; López et al., 2010a; Gao and Horvath, 2014), one of their most important functions being the regulation of arousal and sleep-wake cycle; actually, the lack of OXs or impaired OXR signaling leads to narcolepsy in several animal models (such as mice, rats, and dogs) and humans (Chemelli et al., 1999; Lin et al., 1999; Nishino et al., 2000; Gerashchenko et al., 2001). The fact that BMP8B increased OX expression opens up the possibility that it may have a potential role in the modulation of sleep patterns. We did not address that possibility specifically, but our data show that chronic treatment with BMP8B, specifically within the VMH, tended to increase LA, which may be related to an increase in the arousal state of the animals.

In summary, this study demonstrates that BMP8B modulates energy homeostasis and, more precisely, thermogenesis, via a well-defined hypothalamic pathway involving a VMH-LHA interplay, and it uncovers a functional connection among AMPK in the VMH, glutamatergic signaling, and OX in the LHA. Our results show that two important brain mediators of BAT thermogenesis act in a coordinate network. Whether this mechanism is exclusive for BMP8B or it mediates the effect of other thermogenic factors, such as leptin, thyroid hormones, estradiol, glucagon-like peptide-1, or nicotine, is currently unknown. However, considering that (1) all these factors share the same VMH AMPK-SNS-BAT axis (López et al., 2010b, 2016; Martínez de Morentin et al., 2012, 2014; Whittle et al., 2012; Tanida et al., 2013; Beiroa et al., 2014; Contreras et al., 2015), (2) some of them also modulate the neuronal activity in RPa and IO (López et al., 2010b; Martínez de Morentin et al., 2014), and (3) some regulate OX expression (López et al., 2000; Kane et al., 2000; Porkka-Heiskanen et al., 2004; Pasumarthi et al., 2006), it is tempting to speculate that the AMPK(VMH)-glutamate-OX(LHA)-SNS-BAT axis may be a canonical mechanism to regulate BAT metabolism, with pathophysiological implications in obesity and metabolic disorders.

EXPERIMENTAL PROCEDURES

Animals

Adult female and male Sprague-Dawley rats (200–250 g, Animalario General USC), adult female null *Ox/Hcrt* mice (*orexin/hypocretin*; *B6.129S6-Hcrttm1Ywa/J*, 8–10 weeks old, The Jackson Laboratory), and their WT littermates were used. The animals were housed with an artificial 12-hr light (8:00 a.m. to 8:00 p.m.)/12-hr dark cycle, under controlled temperature and humidity conditions, and they were allowed free access to standard laboratory chow and tap water. During all experimental approaches, the animals were monitored daily for food intake and body weight changes. The experiments were performed in agreement with the International Law on Animal Experimentation and were approved by the USC Ethical Committee (Project ID 15010/14/006).

Experimental Models

Ovariectomy and estradiol replacement, i.c.v. and nucleus-specific treatments, and stereotaxic microinjection of adenoviral and lentiviral vectors were performed as described previously (Nogueiras et al., 2007; López et al., 2008, 2010b; Whittle et al., 2012; Martínez de Morentin et al., 2012, 2014, 2015; Álvarez-Crespo et al., 2013; Imbernon et al., 2013; Contreras et al., 2014; Beiroa et al., 2014; Folgueira et al., 2016). See the Supplemental Experimental Procedures for detailed protocols.

Sample Processing and Analytical Methods

Sample processing, EE, LA, RQ, and nuclear magnetic resonance (NMR) analyses; temperature measurements; in situ hybridization; western blotting; real-time PCR; and immunohistochemistry were performed as described previously (López et al., 2008, 2010b; Whittle et al., 2012; Martínez de Morentin et al., 2012, 2014; Varela et al., 2012; Álvarez-Crespo et al., 2013; Contreras et al., 2014; Beiroa et al., 2014; Folgueira et al., 2016). See the Supplemental Experimental Procedures for detailed protocols.

Statistical Analysis

Data are expressed as mean ± SEM. The mRNA and protein data were expressed in relation (%) to control (vehicle-treated) rats. Error bars represent SEM. Statistical significance was determined by Student's t test when two groups were compared or ANOVA and post hoc two-tailed Bonferroni test when more than two groups were compared ($p < 0.05$ was considered significant).

SUPPLEMENTAL INFORMATION

Supplemental Information includes Supplemental Experimental Procedures, three figures, and one table and can be found with this article online at http://dx.doi.org/10.1016/j.celrep.2016.07.045.

AUTHOR CONTRIBUTIONS

L.M., P.S.-C., C.C., I.G.-G., and N.M.-S. performed the in vivo experiments (hormonal, drug, and viral treatments); the analytical methods (in situ hybridization, western blotting, real-time qPCR, and hormone measurements); and the analysis of temperature, EE, RQ, LA, and NMR, as well as analyzed and collected the data. R.G. performed the immunohistochemistry. L.M., P.S.-C., C.D., R.N., M.T.-S., and M.L. designed the experiments and analyzed, discussed, and interpreted the data. L.M., P.S.-C., and M.L. made the figures. M.L. developed the hypothesis, coordinated and directed the project, and wrote the manuscript. All authors reviewed and edited the manuscript and had final approval of the submitted manuscript.

ACKNOWLEDGMENTS

The research leading to these results received funding from the European Community's Seventh Framework Programme (FP7/2007-2013) under grant agreement 281854 the *ObERStress* project (M.L.), Junta de Andalucía (M.T.-S., P08-CVI-03788 and P12-FQM-01943), Xunta de Galicia (M.L., 2015-CP079; and R.N., 2015-CP080 and PIE13/00024), MINECO co-funded by FEDER (C.D., BFU2014-55871-P; R.N., BFU2015-70664-R; M.T.-S., BFU2014-57581-P; and M.L., SAF2015-71026-R and BFU2015-70454-REDT/Adipoplast). I.G.-G. is a recipient of a fellowship from Ministerio de Educación, Cultura y Deporte (FPU12/01827). CIBER de Fisiopatología de la Obesidad y Nutrición is an initiative of ISCIII. The funders had no role in study design, data collection and analysis, decision to publish, or preparation of the manuscript.

Received: August 7, 2015
Revised: June 16, 2016
Accepted: July 15, 2016
Published: August 11, 2016

REFERENCES

Álvarez-Crespo, M., Martínez-Sánchez, N., Ruíz-Pino, F., Garcia-Lavandeira, M., Alvarez, C.V., Tena-Sempere, M., Nogueiras, R., Diéguez, C., and López, M. (2013). The orexigenic effect of orexin-A revisited: dependence of an intact growth hormone axis. Endocrinology *154*, 3589–3598.

Anand, B.K., and Brobeck, J.R. (1951). Localization of a "feeding center" in the hypothalamus of the rat. Proc. Soc. Exp. Biol. Med. *77*, 323–324.

Beiroa, D., Imbernon, M., Gallego, R., Senra, A., Herranz, D., Villarroya, F., Serrano, M., Fernø, J., Salvador, J., Escalada, J., et al. (2014). GLP-1 agonism

stimulates brown adipose tissue thermogenesis and browning through hypothalamic AMPK. Diabetes *63*, 3346–3358.

Bowers, R.R., Kim, J.W., Otto, T.C., and Lane, M.D. (2006). Stable stem cell commitment to the adipocyte lineage by inhibition of DNA methylation: role of the BMP-4 gene. Proc. Natl. Acad. Sci. USA *103*, 13022–13027.

Cannon, B., and Nedergaard, J. (2004). Brown adipose tissue: function and physiological significance. Physiol. Rev. *84*, 277–359.

Cerri, M., and Morrison, S.F. (2005). Activation of lateral hypothalamic neurons stimulates brown adipose tissue thermogenesis. Neuroscience *135*, 627–638.

Chemelli, R.M., Willie, J.T., Sinton, C.M., Elmquist, J.K., Scammell, T., Lee, C., Richardson, J.A., Williams, S.C., Xiong, Y., Kisanuki, Y., et al. (1999). Narcolepsy in orexin knockout mice: molecular genetics of sleep regulation. Cell *98*, 437–451.

Contreras, C., González-García, I., Martínez-Sánchez, N., Seoane-Collazo, P., Jacas, J., Morgan, D.A., Serra, D., Gallego, R., González, F., Casals, N., et al. (2014). Central ceramide-induced hypothalamic lipotoxicity and ER stress regulate energy balance. Cell Rep. *9*, 366–377.

Contreras, C., González, F., Fernø, J., Diéguez, C., Rahmouni, K., Nogueiras, R., and López, M. (2015). The brain and brown fat. Ann. Med. *47*, 150–168.

Cypess, A.M., Lehman, S., Williams, G., Tal, I., Rodman, D., Goldfine, A.B., Kuo, F.C., Palmer, E.L., Tseng, Y.H., Doria, A., et al. (2009). Identification and importance of brown adipose tissue in adult humans. N. Engl. J. Med. *360*, 1509–1517.

Fliers, E., Klieverik, L.P., and Kalsbeek, A. (2010). Novel neural pathways for metabolic effects of thyroid hormone. Trends Endocrinol. Metab. *21*, 230–236.

Folgueira, C., Beiroa, D., Callon, A., Al-Massadi, O., Barja-Fernandez, S., Senra, A., Fernø, J., López, M., Dieguez, C., Casanueva, F.F., et al. (2016). Uroguanylin action in the brain reduces weight gain in obese mice via different efferent autonomic pathways. Diabetes *65*, 421–432.

Gao, X.B., and Horvath, T. (2014). Function and dysfunction of hypocretin/orexin: an energetics point of view. Annu. Rev. Neurosci. *37*, 101–116.

Gerashchenko, D., Kohls, M.D., Greco, M., Waleh, N.S., Salin-Pascual, R., Kilduff, T.S., Lappi, D.A., and Shiromani, P.J. (2001). Hypocretin-2-saporin lesions of the lateral hypothalamus produce narcoleptic-like sleep behavior in the rat. J. Neurosci. *21*, 7273–7283.

Grefhorst, A., van den Beukel, J.C., van Houten, E.L., Steenbergen, J., Visser, J.A., and Themmen, A.P. (2015). Estrogens increase expression of bone morphogenetic protein 8b in brown adipose tissue of mice. Biol. Sex Differ. *6*, 7.

Hecherington, A., and Ranson, S. (1942). The spontaneous activity and food intake of rats with hypothalamic lesions. Am. J. Physiol. *136*, 609–617.

Huang, H., Song, T.J., Li, X., Hu, L., He, Q., Liu, M., Lane, M.D., and Tang, Q.Q. (2009). BMP signaling pathway is required for commitment of C3H10T1/2 pluripotent stem cells to the adipocyte lineage. Proc. Natl. Acad. Sci. USA *106*, 12670–12675.

Imbernon, M., Beiroa, D., Vázquez, M.J., Morgan, D.A., Veyrat-Durebex, C., Porteiro, B., Díaz-Arteaga, A., Senra, A., Busquets, S., Velásquez, D.A., et al. (2013). Central melanin-concentrating hormone influences liver and adipose metabolism via specific hypothalamic nuclei and efferent autonomic/JNK1 pathways. Gastroenterology *144*, 636–649.e6.

Jia, X., Yan, J., Xia, J., Xiong, J., Wang, T., Chen, Y., Qi, A., Yang, N., Fan, S., Ye, J., and Hu, Z. (2012). Arousal effects of orexin A on acute alcohol intoxication-induced coma in rats. Neuropharmacology *62*, 775–783.

Kane, J.K., Parker, S.L., Matta, S.G., Fu, Y., Sharp, B.M., and Li, M.D. (2000). Nicotine up-regulates expression of orexin and its receptors in rat brain. Endocrinology *141*, 3623–3629.

Kim, K.W., Zhao, L., Donato, J., Jr., Kohno, D., Xu, Y., Elias, C.F., Lee, C., Parker, K.L., and Elmquist, J.K. (2011). Steroidogenic factor 1 directs programs regulating diet-induced thermogenesis and leptin action in the ventral medial hypothalamic nucleus. Proc. Natl. Acad. Sci. USA *108*, 10673–10678.

Kuo, M.M., Kim, S., Tseng, C.Y., Jeon, Y.H., Choe, S., and Lee, D.K. (2014). BMP-9 as a potent brown adipogenic inducer with anti-obesity capacity. Biomaterials *35*, 3172–3179.

Lin, L., Faraco, J., Li, R., Kadotani, H., Rogers, W., Lin, X., Qiu, X., de Jong, P.J., Nishino, S., and Mignot, E. (1999). The sleep disorder canine narcolepsy is caused by a mutation in the hypocretin (orexin) receptor 2 gene. Cell *98*, 365–376.

Lindberg, D., Chen, P., and Li, C. (2013). Conditional viral tracing reveals that steroidogenic factor 1-positive neurons of the dorsomedial subdivision of the ventromedial hypothalamus project to autonomic centers of the hypothalamus and hindbrain. J. Comp. Neurol. *521*, 3167–3190.

López, M., Seoane, L., García, M.C., Lago, F., Casanueva, F.F., Señarís, R., and Diéguez, C. (2000). Leptin regulation of prepro-orexin and orexin receptor mRNA levels in the hypothalamus. Biochem. Biophys. Res. Commun. *269*, 41–45.

López, M., Lage, R., Saha, A.K., Pérez-Tilve, D., Vázquez, M.J., Varela, L., Sangiao-Alvarellos, S., Tovar, S., Raghay, K., Rodríguez-Cuenca, S., et al. (2008). Hypothalamic fatty acid metabolism mediates the orexigenic action of ghrelin. Cell Metab. *7*, 389–399.

López, M., Tena-Sempere, M., and Diéguez, C. (2010a). Cross-talk between orexins (hypocretins) and the neuroendocrine axes (hypothalamic-pituitary axes). Front. Neuroendocrinol. *31*, 113–127.

López, M., Varela, L., Vázquez, M.J., Rodríguez-Cuenca, S., González, C.R., Velagapudi, V.R., Morgan, D.A., Schoenmakers, E., Agassandian, K., Lage, R., et al. (2010b). Hypothalamic AMPK and fatty acid metabolism mediate thyroid regulation of energy balance. Nat. Med. *16*, 1001–1008.

López, M., Alvarez, C.V., Nogueiras, R., and Diéguez, C. (2013). Energy balance regulation by thyroid hormones at central level. Trends Mol. Med. *19*, 418–427.

López, M., Nogueiras, R., Tena-Sempere, M., and Diéguez, C. (2016). Hypothalamic AMPK: a canonical regulator of whole-body energy balance. Nat. Rev. Endocrinol. *12*, 421–432.

Madden, C.J., Tupone, D., and Morrison, S.F. (2012). Orexin modulates brown adipose tissue thermogenesis. Biomol. Concepts *3*, 381–386.

Martínez de Morentin, P.B., Whittle, A.J., Fernø, J., Nogueiras, R., Diéguez, C., Vidal-Puig, A., and López, M. (2012). Nicotine induces negative energy balance through hypothalamic AMP-activated protein kinase. Diabetes *61*, 807–817.

Martínez de Morentin, P.B., González-García, I., Martins, L., Lage, R., Fernández-Mallo, D., Martínez-Sánchez, N., Ruíz-Pino, F., Liu, J., Morgan, D.A., Pinilla, L., et al. (2014). Estradiol regulates brown adipose tissue thermogenesis via hypothalamic AMPK. Cell Metab. *20*, 41–53.

Martínez de Morentin, P.B., Lage, R., González-García, I., Ruíz-Pino, F., Martins, L., Fernández-Mallo, D., Gallego, R., Fernø, J., Señarís, R., Saha, A.K., et al. (2015). Pregnancy induces resistance to the anorectic effect of hypothalamic malonyl-CoA and the thermogenic effect of hypothalamic AMPK inhibition in female rats. Endocrinology *156*, 947–960.

Mauvais-Jarvis, F. (2015). Sex differences in metabolic homeostasis, diabetes, and obesity. Biol. Sex Differ. *6*, 14.

Modica, S., and Wolfrum, C. (2013). Bone morphogenic proteins signaling in adipogenesis and energy homeostasis. Biochim. Biophys. Acta *1831*, 915–923.

Morrison, S.F., Madden, C.J., and Tupone, D. (2012). An orexinergic projection from perifornical hypothalamus to raphe pallidus increases rat brown adipose tissue thermogenesis. Adipocyte *1*, 116–120.

Morrison, S.F., Madden, C.J., and Tupone, D. (2014). Central neural regulation of brown adipose tissue thermogenesis and energy expenditure. Cell Metab. *19*, 741–756.

Nedergaard, J., Bengtsson, T., and Cannon, B. (2007). Unexpected evidence for active brown adipose tissue in adult humans. Am. J. Physiol. Endocrinol. Metab. *293*, E444–E452.

Nishino, S., Ripley, B., Overeem, S., Lammers, G.J., and Mignot, E. (2000). Hypocretin (orexin) deficiency in human narcolepsy. Lancet *355*, 39–40.

Nogueiras, R., Wiedmer, P., Perez-Tilve, D., Veyrat-Durebex, C., Keogh, J.M., Sutton, G.M., Pfluger, P.T., Castaneda, T.R., Neschen, S., Hofmann, S.M., et al. (2007). The central melanocortin system directly controls peripheral lipid metabolism. J. Clin. Invest. *117*, 3475–3488.

Palmer, B.F., and Clegg, D.J. (2015). The sexual dimorphism of obesity. Mol. Cell. Endocrinol. *402*, 113–119.

Pasumarthi, R.K., Reznikov, L.R., and Fadel, J. (2006). Activation of orexin neurons by acute nicotine. Eur. J. Pharmacol. *535*, 172–176.

Perkins, M.N., Rothwell, N.J., Stock, M.J., and Stone, T.W. (1981). Activation of brown adipose tissue thermogenesis by the ventromedial hypothalamus. Nature *289*, 401–402.

Porkka-Heiskanen, T., Kalinchuk, A., Alanko, L., Huhtaniemi, I., and Stenberg, D. (2004). Orexin A and B levels in the hypothalamus of female rats: the effects of the estrous cycle and age. Eur. J. Endocrinol. *150*, 737–742.

Qian, S.W., Tang, Y., Li, X., Liu, Y., Zhang, Y.Y., Huang, H.Y., Xue, R.D., Yu, H.Y., Guo, L., Gao, H.D., et al. (2013). BMP4-mediated brown fat-like changes in white adipose tissue alter glucose and energy homeostasis. Proc. Natl. Acad. Sci. USA *110*, E798–E807.

Rosin, D.L., Weston, M.C., Sevigny, C.P., Stornetta, R.L., and Guyenet, P.G. (2003). Hypothalamic orexin (hypocretin) neurons express vesicular glutamate transporters VGLUT1 or VGLUT2. J. Comp. Neurol. *465*, 593–603.

Schneeberger, M., Gomis, R., and Claret, M. (2014). Hypothalamic and brainstem neuronal circuits controlling homeostatic energy balance. J. Endocrinol. *220*, T25–T46.

Schulz, T.J., and Tseng, Y.H. (2009). Emerging role of bone morphogenetic proteins in adipogenesis and energy metabolism. Cytokine Growth Factor Rev. *20*, 523–531.

Sellayah, D., and Sikder, D. (2012). Orexin receptor-1 mediates brown fat developmental differentiation. Adipocyte *1*, 58–63.

Sellayah, D., and Sikder, D. (2014). Orexin restores aging-related brown adipose tissue dysfunction in male mice. Endocrinology *155*, 485–501.

Sellayah, D., Bharaj, P., and Sikder, D. (2011). Orexin is required for brown adipose tissue development, differentiation, and function. Cell Metab. *14*, 478–490.

Stanley, S., Pinto, S., Segal, J., Pérez, C.A., Viale, A., DeFalco, J., Cai, X., Heisler, L.K., and Friedman, J.M. (2010). Identification of neuronal subpopulations that project from hypothalamus to both liver and adipose tissue polysynaptically. Proc. Natl. Acad. Sci. USA *107*, 7024–7029.

Tang, Q.Q., Otto, T.C., and Lane, M.D. (2004). Commitment of C3H10T1/2 pluripotent stem cells to the adipocyte lineage. Proc. Natl. Acad. Sci. USA *101*, 9607–9611.

Tanida, M., Yamamoto, N., Shibamoto, T., and Rahmouni, K. (2013). Involvement of hypothalamic AMP-activated protein kinase in leptin-induced sympathetic nerve activation. PLoS ONE *8*, e56660.

Teske, J.A., Levine, A.S., Kuskowski, M., Levine, J.A., and Kotz, C.M. (2006). Elevated hypothalamic orexin signaling, sensitivity to orexin A, and spontaneous physical activity in obesity-resistant rats. Am. J. Physiol. Regul. Integr. Comp. Physiol. *291*, R889–R899.

Tong, Q., Ye, C., McCrimmon, R.J., Dhillon, H., Choi, B., Kramer, M.D., Yu, J., Yang, Z., Christiansen, L.M., Lee, C.E., et al. (2007). Synaptic glutamate release by ventromedial hypothalamic neurons is part of the neurocircuitry that prevents hypoglycemia. Cell Metab. *5*, 383–393.

Townsend, K.L., Suzuki, R., Huang, T.L., Jing, E., Schulz, T.J., Lee, K., Taniguchi, C.M., Espinoza, D.O., McDougall, L.E., Zhang, H., et al. (2012). Bone morphogenetic protein 7 (BMP7) reverses obesity and regulates appetite through a central mTOR pathway. FASEB J. *26*, 2187–2196.

Townsend, K.L., An, D., Lynes, M.D., Huang, T.L., Zhang, H., Goodyear, L.J., and Tseng, Y.H. (2013). Increased mitochondrial activity in BMP7-treated brown adipocytes, due to increased CPT1- and CD36-mediated fatty acid uptake. Antioxid. Redox Signal. *19*, 243–257.

Tseng, Y.H., Kokkotou, E., Schulz, T.J., Huang, T.L., Winnay, J.N., Taniguchi, C.M., Tran, T.T., Suzuki, R., Espinoza, D.O., Yamamoto, Y., et al. (2008). New role of bone morphogenetic protein 7 in brown adipogenesis and energy expenditure. Nature *454*, 1000–1004.

Tsujino, N., and Sakurai, T. (2009). Orexin/hypocretin: a neuropeptide at the interface of sleep, energy homeostasis, and reward system. Pharmacol. Rev. *61*, 162–176.

Tupone, D., Madden, C.J., Cano, G., and Morrison, S.F. (2011). An orexinergic projection from perifornical hypothalamus to raphe pallidus increases rat brown adipose tissue thermogenesis. J. Neurosci. *31*, 15944–15955.

van Marken Lichtenbelt, W.D., Vanhommerig, J.W., Smulders, N.M., Drossaerts, J.M., Kemerink, G.J., Bouvy, N.D., Schrauwen, P., and Teule, G.J. (2009). Cold-activated brown adipose tissue in healthy men. N. Engl. J. Med. *360*, 1500–1508.

Varela, L., Martínez-Sánchez, N., Gallego, R., Vázquez, M.J., Roa, J., Gándara, M., Schoenmakers, E., Nogueiras, R., Chatterjee, K., Tena-Sempere, M., et al. (2012). Hypothalamic mTOR pathway mediates thyroid hormone-induced hyperphagia in hyperthyroidism. J. Pathol. *227*, 209–222.

Villarroya, F., and Vidal-Puig, A. (2013). Beyond the sympathetic tone: the new brown fat activators. Cell Metab. *17*, 638–643.

Virtanen, K.A., Lidell, M.E., Orava, J., Heglind, M., Westergren, R., Niemi, T., Taittonen, M., Laine, J., Savisto, N.J., Enerbäck, S., and Nuutila, P. (2009). Functional brown adipose tissue in healthy adults. N. Engl. J. Med. *360*, 1518–1525.

Whittle, A.J., Carobbio, S., Martíns, L., Slawik, M., Hondares, E., Vázquez, M.J., Morgan, D., Csikasz, R.I., Gallego, R., Rodriguez-Cuenca, S., et al. (2012). BMP8B increases brown adipose tissue thermogenesis through both central and peripheral actions. Cell *149*, 871–885.

Xu, Y., Nedungadi, T.P., Zhu, L., Sobhani, N., Irani, B.G., Davis, K.E., Zhang, X., Zou, F., Gent, L.M., Hahner, L.D., et al. (2011). Distinct hypothalamic neurons mediate estrogenic effects on energy homeostasis and reproduction. Cell Metab. *14*, 453–465.

Yasuda, T., Masaki, T., Kakuma, T., Hara, M., Nawata, T., Katsuragi, I., and Yoshimatsu, H. (2005). Dual regulatory effects of orexins on sympathetic nerve activity innervating brown adipose tissue in rats. Endocrinology *146*, 2744–2748.

Yeo, G.S., and Heisler, L.K. (2012). Unraveling the brain regulation of appetite: lessons from genetics. Nat. Neurosci. *15*, 1343–1349.

Ziegler, D.R., Cullinan, W.E., and Herman, J.P. (2002). Distribution of vesicular glutamate transporter mRNA in rat hypothalamus. J. Comp. Neurol. *448*, 217–229.

Cell Reports, Volume *16*

Supplemental Information

A Functional Link between AMPK and Orexin Mediates the Effect of BMP8B on Energy Balance

Luís Martins, Patricia Seoane-Collazo, Cristina Contreras, Ismael González-García, Noelia Martínez-Sánchez, Francisco González, Juan Zalvide, Rosalía Gallego, Carlos Diéguez, Rubén Nogueiras, Manuel Tena-Sempere, and Miguel López

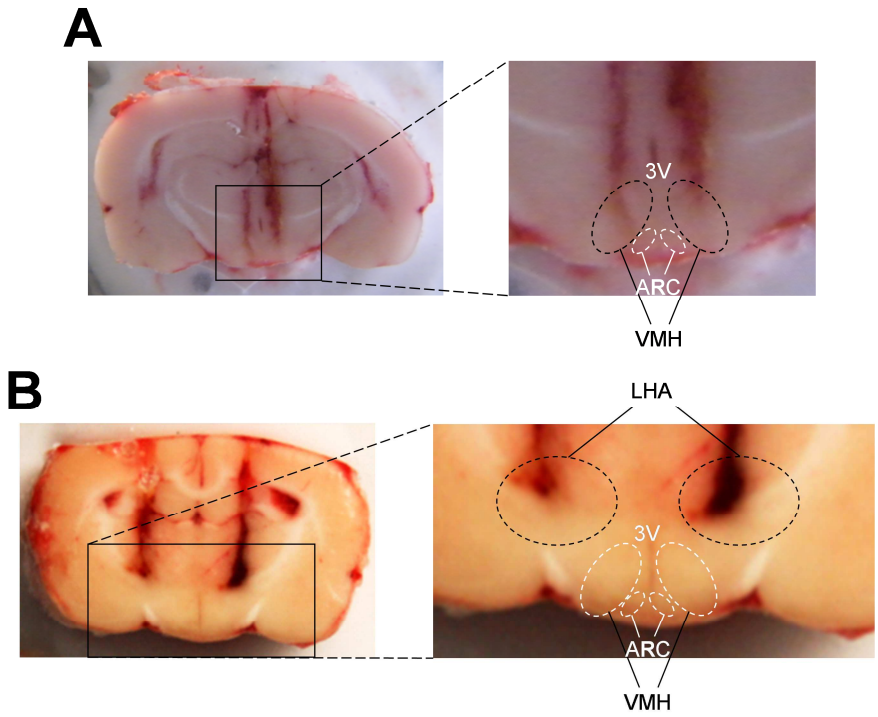

FIGURE S1 related to Figure 2. Anatomical validation of VMH and LHA injections
Coronal sections of rat brains showing the localization of the cannulae in the VMH **(A)** and the LHA **(B).**

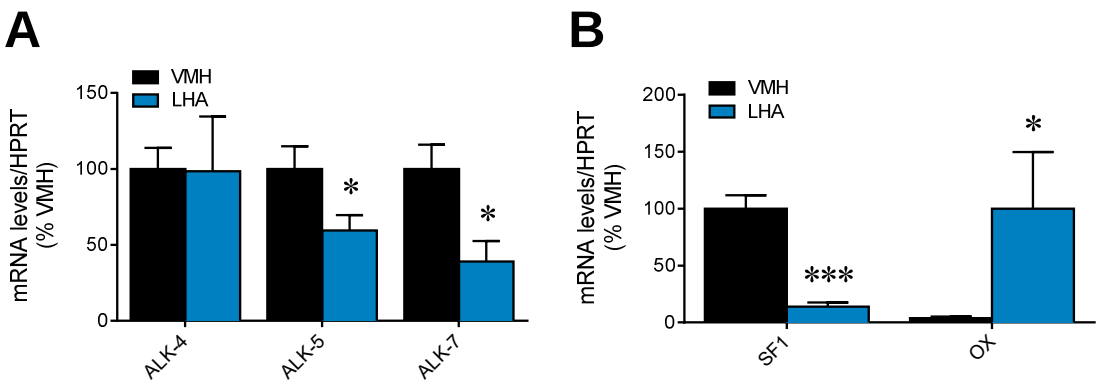

FIGURE S2 related to Figure 2. Hypothalamic expression of BMP8B Type I receptors
(A) mRNA expression of BMP8B Type I receptors . Data are expressed as mean ± SEM; n=4-6 animals per experimental group. * and *** P<0.01 and 0.001 *vs.* VMH, # P<0.05 *vs.* LHA.

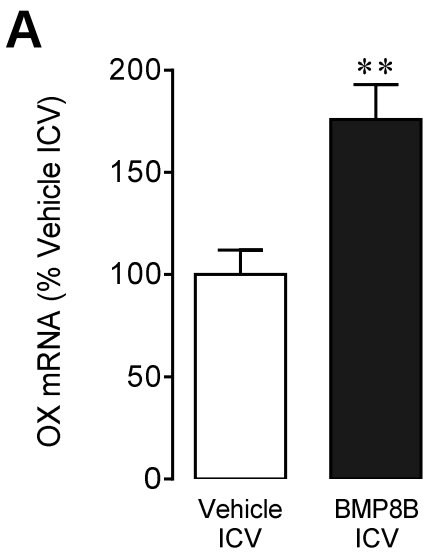

FIGURE S3 related to Figure 4. Effect of central administration of BMP8B on OX in the LHA

(A) OX mRNA levels in the LHA of rats receiving ICV administration of vehicle of BMP8B. Data are expressed as mean ± SEM; n=8 animals per experimental group. ** P<0.01 *vs.* vehicle

Table S1 related to Figures 3 and S2: Primers and probes for real-time PCR (TaqMan®) analysis

mRNA	GenBank Accession Number		Sequence
ALK-4	NM_199230.1	Assay ID	ThermoFisher TaqMan® Gene Expression Assays Assay ID Rn01761726_m1
ALK-5	NM_012775.2	Assay ID	ThermoFisher TaqMan® Gene Expression Assays Assay ID Rn00688966_m1
ALK-7	NM_139090.1	Assay ID	ThermoFisher TaqMan® Gene Expression Assays Assay ID Rn00594657_m1
CIDEA	NM_001170467.1	Assay ID	ThermoFisher TaqMan® Gene Expression Assays Assay ID Rn04181355_m1
FABP3	NM_024162.1	Fw Primer Rv Primer Probe	5'-ACGGAGGCAAACTGGTCCAT-3' 5'-CACTTAGTTCCCGTGTAAGCGTAGTC-3' FAM-5'-TGCAGAAGTGGGACGGGCAGG-3'-TAMRA
HPRT	NM_012583	Fw Primer Rv Primer Probe	5'-AGCCGACCGGTTCTGTCAT-3' 5'-GGTCATAACCTGGTTCATCATCAC -3' FAM-5'- CGACCCTCAGTCCCAGCGTCGTGAT 3'-TAMRA
PGC1α	NM_031347	Fw Primer Rv Primer Probe	5'-CGATCACCATATTCCAGGTCAAG-3' 5'-CGATGTGTGCGGTGTCTGTAGT -3' 5'-AGGTCCCCAGGCAGTAGATCCTCTTCAAGA -3'
PGC1β	NM_176075	Assay ID	ThermoFisher TaqMan® Gene Expression Assays Assay ID Rn00598552_m1
PRDM16	XM_008764418.1	Assay ID	ThermoFisher TaqMan® Gene Expression Assays Assay ID Mm01266512_m1
UCP1	NM_012682	Fw Primer Rv Primer Probe	5'-CAATGACCATGTACACCAAGGAA-3' 5'-GATCCGAGTCGCAGAAAAGAA-3' FAM-5'-ACCGGCAGCCTTTTTCAAAGGGTTTG-3'-TAMRA
UCP3	NM_003356.3	Assay ID	ThermoFisher TaqMan® Gene Expression Assays Assay ID Rn00565874_m1

SUPPLEMENTAL EXPERIMENTAL PROCEDURES

Ovariectomy and estradiol replacement

Sprague-Dawley rats were bilaterally ovariectomized (OVX) or sham-operated as described previously (Martínez de Morentin et al., 2014; Martinez de Morentin et al., 2015). Estradiol treatment was carried out three weeks after surgery to ensure a total washout of endogenous ovarian hormones. OVX rats received a daily SC injection of estradiol (estradiol benzoate; 2 µg dissolved in 100 µL of sesame oil; both from *Sigma;* St Louis, MO, USA) or vehicle (100 µL of sesame oil; control rats) during 3 days (Martínez de Morentin et al., 2014; Martinez de Morentin et al., 2015).

Intracerebroventricular and nucleus-specific treatments

ICV cannulae were implanted under ketamine/xylazine anesthesia, as previously described (Nogueiras et al., 2007; López et al., 2008; López et al., 2010; Whittle et al., 2012; Martínez de Morentin et al., 2012; Imbernon et al., 2013; Martínez de Morentin et al., 2014; Contreras et al., 2014; Beiroa et al., 2014). Animals were individually caged and allowed to recover for four days. For BMP8B acute experiments, animals were ICV treated with vehicle (5 µL of saline for rats and 2 µL of saline for mice) or BMP8B (5 µL of 4nM BMP8B for rats and 2 µL of 100 pM BMP8B for mice) (*R&D Systems*, Minneapolis, MN, USA); animals were treated at 09:00 AM (one hour after the light cycle had commenced). For the cold exposure experiments female rats (experiments were repeated twice and the number of animals per experimental group was 4-8 in each replicate, a representative experiment is shown) or mice (the number of animals per experimental group was 6-8) were housed in a climate chamber at 4ºC. BMP8B was

ICV administered (at the above dose) after 10 hours and maintained the animals in a cold environment for a total 12 hours.

For the experiment with the selective orexin 1 receptor (OX1R) antagonist, rats received an ICV injection of vehicle (5 μL of DMSO; *Sigma*; St Louis, MO, USA) or SB-334867 (10 nmol in 5μL; *Tocris Bioscience*; Bristol, UK) (Jia et al., 2012) 30 minutes prior to BMP8B administration. The experiments were repeated five times and the number of animals per experimental group was 6-8 in each of replicate (total number of animals of 30-40 per experimental group).

For chronic treatments, BMP8B (0.1 pmol/day/rat) was delivered via a permanent 28-gauge stainless steel cannula (*Plastics One*, Roanoke, VA, USA) inserted bilaterally either in VMH or LHA, directed to the following stereotaxic coordinates: 2.8 mm posterior to bregma, ±0.6 mm lateral to midline and 10.1 mm ventral or 2.9 mm posterior to bregma, ±2.0 mm lateral to midline and 8.1 mm ventral, respectively (Imbernon et al., 2013; Contreras et al., 2014). A catheter tube was connected from each infusion cannula to an osmotic minipump flow moderator (Model 1007D; *Alzet Osmotic Pumps*, Cupertino, CA, USA). These pumps had a flow rate of 0,5 μL/hour during 7 days of treatment. The osmotic minipumps were inserted in a subcutaneous pocket on the dorsal surface created using blunt dissection and the treatment was given during 7 days. The experiments were repeated twice and the number of animals per experimental group was 8 in each of replicate (total number of 16 animals per experimental group).

Stereotaxic microinjection of adenoviral and lentiviral vectors

Rats were placed in a stereotaxic frame (*David Kopf Instruments;* Tujunga, CA, USA) under ketamine-xylazine anesthesia. The VMH was targeted bilaterally using a 25-gauge needle (*Hamilton;* Reno, NV, USA). The injections were directed to the

following stereotaxic coordinates for the VMH: 2.4/3.2 mm posterior to the bregma (two injections were performed in each VMH), ±0.6 mm lateral to midline and 10.1 mm ventral as previously reported (López et al., 2008; López et al., 2010; Whittle et al., 2012; Martínez de Morentin et al., 2012; Martínez de Morentin et al., 2014; Contreras et al., 2014; Beiroa et al., 2014). Adenoviral vectors (*Viraquest;* North Liberty, IA, USA) containing green fluorescence protein (GFP, used as control) or a constitutive active isoform of AMPKα (AMPKα-CA) (wild-type, at 10^{12} pfu/ml) were delivered at a rate of 200 nl/min for 5 min (1 µl/injection site) as previously reported (López et al., 2008; López et al., 2010; Whittle et al., 2012; Martínez de Morentin et al., 2012; Martínez de Morentin et al., 2014; Contreras et al., 2014; Beiroa et al., 2014). Animals were treated with BMP8B during 2 hours. The experiment was repeated twice and the number of animals per experimental group was 6 in each replicate (total number of 12 animals per experimental group).

Lentiviral vectors (*Sigma;* St. Louis, MO, USA) containing green fluorescence protein (TurboGFP (SHC003V, used as control) or a shRNA targeting VGLUT2 (at 10^6 TU/ml) were delivered at the LHA (2.9 mm posterior to bregma, ±2.0 mm lateral to midline and 8.1 mm ventral). Animals were treated 28 days prior to BMP8B ICV treatment that lasted 2 hours. The number of animals per experimental group was 9.

Energy expenditure, locomotor activity, respiratory quotient and nuclear magnetic resonance analysis

Rats were analyzed for EE, RQ and LA using a calorimetric system (*LabMaster; TSE Systems;* Bad Homburg, Germany), as previously shown (Nogueiras et al., 2007; Martínez de Morentin et al., 2012; Imbernon et al., 2013; Martínez de Morentin et al., 2014). Rats were placed for adaptation for 1 week before starting the measurements. For

the measurement of body composition, we used NMR imaging (*Whole Body Composition Analyzer; EchoMRI;* Houston, TX), as previously shown (Martínez de Morentin et al., 2012; Imbernon et al., 2013; Martínez de Morentin et al., 2014). We used 8 animals per experimental group.

Temperature measurements

Body temperature was recorded twice at the beginning and the end of the treatments with a rectal probe connected to digital thermometer (*BAT-12 Microprobe-Thermometer; Physitemp*; NJ, USA). Skin temperature surrounding BAT was recorded with an infrared camera (*B335 Thermal Imaging Camera; FLIR*; West Malling, Kent, UK) (Whittle et al., 2012; Martínez de Morentin et al., 2012; Martínez de Morentin et al., 2014; Contreras et al., 2014; Beiroa et al., 2014).

Sample processing

Rats and mice were killed by cervical dislocation. From each animal, either the whole brain (for *in situ* hybridization) or the VMH and LHA (dissected from the whole hypothalamus for RT-PCR or western blot), as well as the BAT (for western blot) were harvested and immediately homogenized on ice to preserve phosphorylated protein levels. Samples were stored at -80ºC until further processing. Dissection of the VMH and LHA was performed by micropunches under the microscope, as previously shown (López et al., 2010; Whittle et al., 2012; Martínez de Morentin et al., 2014; Contreras et al., 2014; Beiroa et al., 2014). The specificity of the VMH and LHA dissections was confirmed by analyzing the mRNA of steroidogenic factor-1 and prepro- orexin **(Figure S2B).**

In situ hybridization

Coronal brain sections (16 μm) were probed with a specific oligonucleotide for prepro-OX (*GenBank Accession Number*: NM_013179; 5'-TTC GTA GAG ACG GCA GGA ACA CGT CTT CTG GCG ACA-3') as previously published (López et al., 2008; López et al., 2010; Whittle et al., 2012; Martínez de Morentin et al., 2012; Álvarez-Crespo et al., 2013; Martínez de Morentin et al., 2014). Sections were scanned and the hybridization signal was quantified by densitometry using *ImageJ-1.33* software (*NIH*, Bethesda, MD, USA). We used 6-8 animals per experimental group and 16-20 sections for each animal (4-5 slides with four sections per slide). The mean of these 16-20 values was used as densitometry value for each animal.

Western Blotting

VMH, LHA and BAT protein lysates were subjected to SDS-PAGE, electrotransferred on a PVDF membrane and probed with the following antibodies: AMPKα1, AMPKα2 (Millipore, Billerica, MA, USA); FAS (*BD*; Franklin Lakes, NJ, USA), ACC, pACC-Ser^{79}, pAMPK-Thr^{172} (*Cell Signaling;* Danvers; MA, USA); α-tubulin, β-actin (*Sigma;* St. Louis, MO, USA); VGLUT2 and UCP1 (*Abcam*; Cambridge, UK) as previously described (López et al., 2008; López et al., 2010; Whittle et al., 2012; Martínez de Morentin et al., 2012; Martínez de Morentin et al., 2014; Contreras et al., 2014; Beiroa et al., 2014). Values were expressed in relation to α-tubulin (for BAT) or β-actin (for VMH and LHA) protein levels. We used 4-8 animals per experimental group.

Real-time PCR

We perform real-time PCR (*TaqMan®*; *Applied Biosystems*; Carlsbad, CA, USA) as previously described (López et al., 2010; Whittle et al., 2012; Martínez de Morentin et al., 2012; Martínez de Morentin et al., 2014) using specific sets of primers and probes **(Table S1)**. Values were expressed relative to Hypoxanthine-guanine phosphoribosyltransferase (HPRT) levels. We used 8-9 animals per experimental group.

Immunohistochemistry

Detection of UCP1 in WAT was performed using anti-UCP1 (1:500; *Abcam*, Cambridge, UK). Detection was done with an anti-rabbit antibody conjugated with Alexa 488 (1:200; *Molecular Probes*; Grand Island, NY, US) as previously reported (Folgueira et al., 2016). Detection of GFP was performed with an immunofluorescence procedure, using a rabbit anti-GFP (1:200; *Abcam*; Cambridge, UK). Detection was done with an anti-rabbit antibody conjugated with *Alexa 488* (1:200; *Molecular Probes;* Grand Island, NY, US) as previously reported (López et al., 2008; López et al., 2010; Varela et al., 2012; Whittle et al., 2012; Imbernon et al., 2013). Images were taken with a digital camera *Olympus XC50* (*Olympus Corporation*, Tokyo, Japan) at 20X. Digital images were quantified with ImageJ Software (*National Institutes of Health*, USA).

SUPPLEMENTAL REFERENCES

Álvarez-Crespo,M., Martinez-Sanchez,N., Ruiz-Pino,F., Garcia-Lavandeira,M., Alvarez,C.V., Tena-Sempere,M., Nogueiras,R., Diéguez,C., and López,M. (2013). The orexigenic effect of orexin-A revisited: dependence of an intact growth hormone axis. Endocrinology *154*, 3589-3598.

Beiroa,D., Imbernon,M., Gallego,R., Senra,A., Herranz,D., Villaroya,F., Serrano,M., Ferno,J., Salvador,J., Escalada,J., Dieguez,C., Lopez,M., Fruhbeck,G., and Nogueiras,R. (2014). GLP-1 Agonism Stimulates Brown Adipose Tissue Thermogenesis and Browning Through Hypothalamic AMPK. Diabetes *63*, 3346-3358.

Contreras,C., González-García,I., Martínez-Sánchez,N., Seoane-Collazo,P., Jacas,J., Morgan,D.A., Serra,D., Gallego,R., González,F., Casals,N., Nogueiras,R., Rahmouni,K., Diéguez,C., and López,M. (2014). Central Ceramide-Induced Hypothalamic Lipotoxicity and ER Stress Regulate Energy Balance. Cell Rep. *9*, 366-377.

Folgueira,C., Beiroa,D., Callon,A., Al-Massadi,O., Barja-Fernandez,S., Senra,A., Ferno,J., Lopez,M., Dieguez,C., Casanueva,F.F., Rohner-Jeanrenaud,F., Seoane,L.M., and Nogueiras,R. (2016). Uroguanylin Action in the Brain Reduces Weight Gain in Obese Mice via Different Efferent Autonomic Pathways. Diabetes *65*, 421-432.

Imbernon,M., Beiroa,D., Vazquez,M.J., Morgan,D.A., Veyrat-Durebex,C., Porteiro,B., Diaz-Arteaga,A., Senra,A., Busquets,S., Velasquez,D.A., Al-Massadi,O., Varela,L., Gandara,M., Lopez-Soriano,F.J., Gallego,R., Seoane,L.M., Argiles,J.M., López,M., Davis,R.J., Sabio,G., Rohner-Jeanrenaud,F., Rahmouni,K., Diéguez,C., and Nogueiras,R. (2013). Central Melanin-Concentrating Hormone Influences Liver and Adipose Metabolism Via Specific Hypothalamic Nuclei and Efferent Autonomic/JNK1 Pathways. Gastroenterology *144*, 636-649.

Jia,X., Yan,J., Xia,J., Xiong,J., Wang,T., Chen,Y., Qi,A., Yang,N., Fan,S., Ye,J., and Hu,Z. (2012). Arousal effects of orexin A on acute alcohol intoxication-induced coma in rats. Neuropharmacology *62*, 775-783.

López,M., Lage,R., Saha,A.K., Pérez-Tilve,D., Vázquez,M.J., Varela,L., Sangiao-Alvarellos,S., Tovar,S., Raghay,K., Rodríguez-Cuenca,S., Deoliveira,R.M., Castañeda,T., Datta,R., Dong,J.Z., Culler,M., Sleeman,M.W., Álvarez,C.V., Gallego,R., Lelliott,C.J., Carling,D., Tschop,M.H., Diéguez,C., and Vidal-Puig,A. (2008). Hypothalamic fatty acid metabolism mediates the orexigenic action of ghrelin. Cell Metab *7*, 389-399.

López,M., Varela,L., Vázquez,M.J., Rodríguez-Cuenca,S., González,C.R., Velagapudi,V.R., Morgan,D.A., Schoenmakers,E., Agassandian,K., Lage,R., de Morentin,P.B., Tovar,S., Nogueiras,R., Carling,D., Lelliott,C., Gallego,R., Oresic,M., Chatterjee,K., Saha,A.K., Rahmouni,K., Diéguez,C., and Vidal-Puig,A. (2010). Hypothalamic AMPK and fatty acid metabolism mediate thyroid regulation of energy balance. Nat. Med. *16*, 1001-1008.

Martínez de Morentin,P.B., Gónzalez-García,I., Martins,L., Lage,R., Fernández-Mallo,D., Martínez-Sánchez,N., Ruíz-Pino,F., Liu,J., Morgan,D.A., Pinilla,L., Gallego,R., Saha,A.K., Kalsbeek,A., Fliers,E., Bisschop,P.H., Diéguez,C., Nogueiras,R., Rahmouni,K., Tena-Sempere,M., and López,M. (2014). Estradiol regulates brown adipose tissue thermogenesis via hypothalamic AMPK. Cell Metab *20*, 41-53.

Martinez de Morentin,P.B., Lage,R., Gonzalez-Garcia,I., Ruiz-Pino,F., Martins,L., Fernandez-Mallo,D., Gallego,R., Ferno,J., Senaris,R., Saha,A.K., Tovar,S., Dieguez,C., Nogueiras,R., Tena-Sempere,M., and Lopez,M. (2015). Pregnancy induces resistance to the anorectic effect of hypothalamic malonyl-CoA and the thermogenic effect of hypothalamic AMPK inhibition in female rats. Endocrinology *156*, 947-960.

Martínez de Morentin,P.B., Whittle,A.J., Ferno,J., Nogueiras,R., Diéguez C, Vidal-Puig,A., and López M (2012). Nicotine induces negative energy balance through hypothalamic AMP-activated protein kinase. Diabetes *61*, 807-817.

Nogueiras,R., Wiedmer,P., Perez-Tilve,D., Veyrat-Durebex,C., Keogh,J.M., Sutton,G.M., Pfluger,P.T., Castaneda,T.R., Neschen,S., Hofmann,S.M., Howles,P.N., Morgan,D.A., Benoit,S.C., Szanto,I.,

Schrott,B., Schurmann,A., Joost,H.G., Hammond,C., Hui,D.Y., Woods,S.C., Rahmouni,K., Butler,A.A., Farooqi,I.S., O'rahilly,S., Rohner-Jeanrenaud,F., and Tschop,M.H. (2007). The central melanocortin system directly controls peripheral lipid metabolism. J. Clin. Invest *117*, 3475-3488.

Varela,L., Martínez-Sánchez N., Gallego,R., Vázquez,M.J., Roa,J., Gándara M., Schoenmakers,E., Nogueiras,R., Chatterjee,K., Tena-Sempere,M., Diéguez C, and López M (2012). Hypothalamic mTOR pathway mediates thyroid hormone-induced hyperphagia in hyperthyroidism. J. Pathol. *227*, 209-222.

Whittle,A.J., Carobbio S, Martíns L, Slawik,M., Hondares,E., Vázquez,M.J., Morgan D, Csikasz, RI, Gallego,R., Rodriguez-Cuenca,S., Dale,M., Virtue,S., Villarroya,F., Cannon,B., Rahmouni,K., López M, and Vidal-Puig,A. (2012). Bmp8b increases brown adipose tissue thermogenesis through both central and peripheral actions. Cell *149*, 871-885.